



Application of supersonic ejector principle to enhance flow in low-pressure geothermal production wells

Daniel Wanga Odongo

Thesis of 60 ECTS credits
**Master of Science (M.Sc.) in Sustainable Energy
Engineering**

June 2024



Application of supersonic ejector principle to enhance flow in low-pressure geothermal production wells

Thesis of 60 ECTS credits submitted to the School of Science and Engineering
at Reykjavík University in partial fulfillment of
the requirements for the degree of
**Master of Science (M.Sc.) in Sustainable Energy
Engineering**

June 2024

Supervisors:

María Sigríður Guðjónsdóttir, Ph. D.
Associate Professor, Reykjavík University, Iceland

Guðrún Arnbjörg Sævarsdóttir, Ph. D.
Professor, Reykjavík University, Iceland

Ximena Guardia Muguruza
PhD Student, Reykjavík University, Iceland

Examiner:

Ásdís Helgadóttir, Ph. D.
Associate Professor, University of Iceland, Iceland

Copyright
Daniel Wanga Odongo
June 2024

Application of supersonic ejector principle to enhance flow in low-pressure geothermal production wells

Daniel Wanga Odongo

June 2024

Abstract

Geothermal wells are one of the key components and most capital-intensive parts of any geothermal power generation facility. However, they often experience pressure decline over their lifetime, leading in some cases to the well pressure falling below the power plant operating conditions, which make wells unusable for power generation. This can make the overall project more costly since additional wells must be drilled to compensate for the unavailable steam to maintain the desired power plant output. This study explores the possibility of using ejectors to solve that problem. Ejectors have been used in various applications in oil and gas and refrigeration industries. In geothermal power generation, ejectors are widely used to extract non-condensable gases from the condenser. Ejectors are static devices that use kinetic energy from a high-pressure stream to induce flow from a lower-pressure stream. Supersonic ejectors work by using a convergent-divergent nozzle to accelerate a primary fluid to supersonic conditions. This creates an under-pressure that allows a secondary flow to entrain, and the mixture exits at an intermediate pressure. The experiments described in this work were carried out in the Reykjavik University energy laboratory to fabricate and test a supersonic ejector on a laboratory-scale. It was set up to connect two streams of saturated steam at different pressures and compare the results with an analytical model developed in earlier studies. The experiment was focused on the effect of ejector dimensions on performance, specifically the constant area mixing section (CAMS). The experiment was successful in proving that the ejector works by showing gained pressure and entrainment of the secondary flow despite not having a good match with the analytical model. From the experiment, the 5 mm CAMS ejector provided the best results using entrainment ratio, gained pressure and outlet pressure to measure its performance. The analytical model was also used to design a potential supersonic ejector to connect two production wells in the Olkaria geothermal field in Kenya. The design showed that an additional 2.2 MW of electrical power could be generated using this ejector.

Notkun yfirhljóðsútkastarreglu til að auka flæði í lágþrýsti jarðhitavinnsluholum

Daniel Wanga Odongo

júní 2024

Útdráttur

Jarðvarmaborholur eru einn af lykilþáttum fyrir jarðvarmavirkjanir ásamt því að vera einn helsti kostnaðarliður þess. Holurnar tapa hinsvegar oft afli yfir líftíma sinn, sem getur leitt til þess að þrýstingur holanna fer niður fyrir rekstrarþrýsting virkjunarinnar, með þeim afleiðingum að holurnar nýtast ekki til orkuframleiðslu. Þetta getur gert heildarverkefnið kostnaðarsamara þar sem bora þarf viðbótarholur sem vega upp á móti minnkandi gufufurframleiðslu og til að viðhalda æskilegum afköstum virkjunarinnar. Þeysar hafa verið notaðir við ýmsar aðstæður í olíu, gas- og kæliðnaði. Við orkuframleiðslu í jarðvarmaverum hafa þeysar verið notaðir til þess að ná óþéttanlegum lofftegundum úr eimsvölum. Þeysir er búnaður sem inniheldur enga hreyfanlega íhluti og í þeim er hreyfiorka frá háþrýstingsflæði notuð til þess að soga inn lágþrýstingsflæði. Í þeysum þar sem flæðið fer yfir hljóðhraða er notaður stútur þar sem endirinn víkkar út (e. convergent-divergent nozzle) til þess að hraða meginflæðinu (e. primary flow) yfir hljóðhraða. Við það myndast undirþrýstingur sem gerir aukaflæðinu (e. secondary flow) kleift að komast inn í þeysinn og blandast við meginflæðið. Blandaða flæðið kemur út við milliprýsting (e. intermediate pressure). Tilraunirnar sem lýst er í þessu verkefni voru framkvæmdar í orkurannsóknarstofu Háskólans í Reykjavík þar sem yfirhljóðhraða þeysir var smíðaður og prófaður á tilraunaskala. Í tilraununum var tveimur straumum af mettaðri gufu við mismunandi þrýsting blandað saman. Niðurstöður tilraunanna voru bornar saman við reiknilíkan sem þróað var úr niðurstöðum úr öðrum verkefnum. Tilraunirnar beindust að því að rannsaka áhrif stærðar ákveðinna hluta þeysanna á virkni þeirra, einna helst þann hluta þeysisins sem er við fast flatarmál þar sem flæðin blandast (e. constant area mixing section, CAMS). Tilraunirnar sýndu góðar niðurstöður fyrir það sem sneri að þrýstingsaukningu (e. gained pressure) og meðsogi (e. entrainment) en samsvöruðu ekki vel við niðurstöður reiknilíkansins. Niðurstöður tilraunanna sýndu fram á að besti þeysirinn var þegar þvermál CAMS var 5 mm, hvað meðsog og þrýstingsaukningu varðar. Reiknilíkanið var einnig notað til að hanna þeysi til að tengja saman flæði úr tveimur vinnsluholum á Olkaria jarðhitasvæðinu í Kenýa. Niðurstöðurnar sýna að mögulegt væri að hækka orkuvinnsluna úr þeim holum um 2.2 MW.

Application of supersonic ejector principle to enhance flow in low-pressure geothermal production wells

Daniel Wanga Odongo

Thesis of 60 ECTS credits submitted to the School of Science and Engineering at Reykjavík University in partial fulfillment of the requirements for the degree of **Master of Science (M.Sc.) in Sustainable Energy Engineering**

June 2024

Student: 
Daniel Wanga Odongo

Supervisors:
María Sigríður Guðjónsdóttir, Ph. D.

Guðrún Arnbjörg Sævarsdóttir, Ph. D.

Ximena Guardia Muguruza

Examiner:
Ásdís Helgadóttir, Ph. D.

The undersigned hereby grants permission to the Reykjavík University Library to reproduce single copies of this Thesis entitled **Application of ejector principle to enhance flow in low-pressure geothermal production wells** and to lend or sell such copies for private, scholarly or scientific research purposes only.

The author reserves all other publication and other rights in association with the copyright in the Thesis, and except as herein before provided, neither the Thesis nor any substantial portion thereof may be printed or otherwise reproduced in any material form whatsoever without the author's prior written permission.

06. June. 2024

.....
date

D.W. Odongo

.....
Daniel Wanga Odongo
Master of Science

I dedicate this work to my late father, who ignited my interest in geothermal studies and has always been my inspiration.

Acknowledgements

My appreciation first to the GRÓ Geothermal Training Program (GRÓ-GTP) for offering me the opportunity and scholarship for my master's studies at Reykjavik University. I would like to thank the director, Guðni Axelsson and GRÓ-GTP staff, Ingimar Haraldsson, and Málfríður Ómarsdóttir for their support. I would also like to thank my classmates and GRÓ GTP fellows who were always there to encourage and support me.

I also recognize the input of my employer, Kenya Electricity Generating Company PLC for giving me the opportunity to study. Special thanks to General Manager, Geothermal Development Mr. Peketsa Mangi, Reservoir and Steamfield Manager Eng. Clety Kwambai and my colleagues for aiding whenever they could.

I would like to thank my supervisors, María Sigríður Guðjónsdóttir, Guðrún Arnbjörg Sævarsdóttir and Ximena Guardia Muguruza for their guidance and mentorship. I also appreciate the input from the rest of the Geojector research project team members, Yonatan Afework Tesfahunegn, Ragnar Lárusson, Jeffrey Macatangay Andal, Egill Júlíusson, Vijay Chauhan, Gunnar Dagur Jónsson, and Hilmar Már Einarsson. I also recognize Gísli Freyr Þorsteinsson, Pétur Freyr Sigurjónsson and Hannes Páll Þórðarson for their assistance during the fabrication of the ejector and the experiments in the Reykjavik University engineering workshop and energy laboratory, I immensely thank them.

Lastly, I would like to thank my family, my mum Colleta, my wife Blanche and our children, Bianca, Dion, and Darren, for their love, patience and understanding.

Preface

This dissertation is an original work by the author, Daniel Wanga Odongo.

Contents

Acknowledgements	xv
Preface	xvii
Contents	xix
List of Figures	xxi
List of Tables	xxiii
List of Abbreviations	xxv
List of Symbols	xxvii
1 Introduction	1
2 Background	3
2.1 Ejector principle	3
2.2 Classification of ejectors	3
2.3 Industrial uses of ejectors	4
2.3.1 Ejector use in refrigeration.	4
2.3.2 Ejector use in steam power plant condensers.....	5
2.3.3 Ejector use in oil and gas.....	6
2.4 Experimental use of ejectors in geothermal wells.....	7
2.5 Computational fluid dynamics analysis for ejectors	8
3 Methodology.....	10
3.1 Analytical model for a supersonic ejector.....	10
3.2 Laboratory experiments	13
3.2.1 Ejector sizing and fabrication.....	13
3.2.2 Laboratory experimental set-up.....	14
3.2.3 Equipment used in the experiment.	15
3.2.4 Experimental procedure	18
4 Results.....	20
4.1 Laboratory experiment results.....	20
4.1.1 Gained pressure.	24
4.1.2 Entrainment ratio.....	25
4.1.3 Area ratio effects	26
4.1.4 Exergy analysis	27
4.2 Comparison of the analytical model and experimental results	28
4.2.1 Entrainment ratio.....	28
4.2.2 Gained pressure	29

4.2.3	Back or outlet pressure	29
4.3	Analytical model application for Olkaria wells	30
4.4	Analytical model results for Olkaria wells.....	31
4.4.1	Exergy analysis	33
5	Discussion	36
6	Conclusion and recommendations	38
6.1	Conclusion.....	38
6.2	Recommendations	38
	Bibliography.....	39
	Appendix A Analytical model equations	41
	Appendix B Ejector fabrication.....	45

List of Figures

Figure 1: Typical ejector profile and parts	3
Figure 2: Ejector operation modes with respect to pressure and entrainment ratio	4
Figure 3: Schematic of ejector refrigeration system.....	5
Figure 4: Profile of ejector for ERS.....	5
Figure 5: Gas extraction system for turbine condensers using SEPS	6
Figure 6: Schematic of APG utilization using a pump and ejector	7
Figure 7: Profile of subsonic ejector for wells ThG-11 and ThG-15 in Theistareykir.....	7
Figure 8: Pressure and velocity profiles for a new proposed supersonic ejector.	8
Figure 9: Profile of supersonic ejector.	11
Figure 10: Supersonic ejector analytical model flow chart.	12
Figure 11: Supersonic ejector dimensions.....	14
Figure 12: Experiment set-up at Reykjavik University energy laboratory.....	15
Figure 13: Flow diagram for the experiment.....	15
Figure 14: Experiment boilers primary.	16
Figure 15: Experiment steam separators.	17
Figure 16: Experiment heat exchanger.....	17
Figure 17: Experimental results for 4 mm CAMS ejector.....	21
Figure 18: Experimental results for 5 mm CAMS ejector.....	22
Figure 19: Experimental results for 7 mm CAMS ejector.....	23
Figure 20: Experimental results for 9 mm CAMS ejector.....	24
Figure 21: Effect of area ratio on gained pressure.....	27
Figure 22: Effect of area ratio on entrainment ratio.	27
Figure 23: Grassman diagram for 5 mm CAMS ejector	28
Figure 24: Map showing wells 905 and 905B on the well pad.	31
Figure 25: Output curves for wells 905 and 905B.....	31
Figure 26: Pressure and velocity profiles for 905 and 905B ejector	33
Figure 27: Grassman diagram for wells 905 and 905B in Olkaria ejector.	34

List of Tables

Table 1: Dimensions for 4, 5, 7 and 9 mm CAMS ejectors used in the experiment	14
Table 2: Measurement devices used in the experiment	18
Table 3: Summary of pressure results from the experiment.....	25
Table 4: Entrainment ratio results from the experiment.....	26
Table 5: Area ratio effects from the experiment	26
Table 6: Experiment and analytical model comparison for entrainment ratio	29
Table 7: Experiment and analytical model comparison for gained pressure.....	29
Table 8: Experiment and analytical model comparison for back pressure.....	29
Table 9: Experiment and analytical model comparison for outlet temperature	30
Table 10: Flow characteristics for wells 905 and 905B in Olkaria	31
Table 11: Analytical model results for wells 905 and 905B	32
Table 12: Performance indicators for wells 905 and 905B ejector	35

List of Abbreviations

AR	Area ratio
CAMS	Constant area mixing section
CFD	Computational fluid dynamics
CV	Control valve
ER	Entrainment ratio
ERS	Ejector refrigeration system
FM	Flow meter
NCG	Non-condensable gases
NXP	Nozzle exit position
PLC	Programmable logic controller
PS	Pressure sensor
RANS	Reynolds-averaged Navier–Stokes
SEPS	Steam ejector pump system
TS	Temperature sensor
VFM	Vortex flow meter
WAG	Water alternated gas

List of Symbols

Symbol	Description	Value/Units
a	Sonic velocity	m/s
A	Area	m^2
c_l	Loss coefficient	-
C_p	Specific heat at constant pressure	kJ/kgK
C_v	Specific heat at constant volume	kJ/kgK
D	Diameter	m
e	Specific exergy	kJ/kg
E	Total exergy	kJ
h	Enthalpy	kJ/kg
k	Ratio of specific heats	-
\dot{m}	Mass flow rate	kg/s
p	Pressure	bar-g
s	Specific entropy	kJ/kgK
T	Temperature	$^{\circ}\text{C}$
v	Fluid velocity	m/s
ρ	Density	kg/m^3
η_n	Nozzle isentropic efficiency	-
η_{ex}	Exergy efficiency	-

Subscripts

1	Primary inlet
2	Nozzle throat
3	Point between the nozzle exit and hypothetical throat
4	Primary flow at hypothetical throat
5	Secondary inlet
6	Entrained flow at the hypothetical throat
7	Constant area mixing section inlet
8	Shockwave inside the constant area mixing section
9	Diffuser exit / Ejector outlet
*	Critical values at sonic point
p	Primary
s	Secondary
c	Combined
o	Outlet

Chapter 1

Introduction

In the development and operation of a geothermal power generation facility, geothermal wells drilling is considered one of the most capital-intensive activities. Estimates of 34% of the total investment cost has been reported for the drilling of production wells for a 50 MW plant geothermal power plant [1]. After they are drilled and connected, the wells naturally decline in output over their lifetime to the extent that the pressure sometimes falls below the steam gathering system pressure and cannot be used for power generation. Such wells are normally shut or reused for other purposes like reinjection and monitoring. However, as the power generation must be maintained, additional wells, referred to as make-up wells, must be drilled and connected to offset this reduced output. This increases the already high drilling costs, and costs of additional infrastructure like well pads, roads, and buildings.

Ejectors are devices that can be used to combine two flow streams at different pressures by accelerating a primary fluid to a higher velocity that creates an under-pressure thereby allowing a secondary lower pressure fluid to entrain, mix with the primary and exit at an intermediate pressure higher than the secondary flow pressure. These devices have the potential to connect low-pressure wells to a higher-pressure steam gathering system for power generation, reducing the need for drilling make-up wells. This could reduce the capital-intensive costs of drilling and, therefore, reduce investment and maintenance costs for geothermal power generation projects.

Ejectors offer an advantage considering that they do not have moving mechanical parts and therefore require minimal servicing or maintenance work. They can also be used with a wide range of fluids [2]. In addition, they do not require power as an input to function.

Ejectors can be classified as subsonic or supersonic. Subsonic ejectors refer to ejectors where the primary flow is accelerated through a convergent nozzle to a velocity lower than Mach 1 (velocity of sound in a gas). Supersonic ejectors on the other hand use a convergent-divergent nozzle to accelerate the flow to above Mach 1. Supersonic ejectors are considered more effective since higher velocity and shockwaves creates more under-pressure and higher entrainment of the secondary fluid. The higher kinetic energy also make them have a higher downstream pressure than the subsonic ones after the diffuser section. The choice of using a supersonic or subsonic ejector is made based on the difference in pressure between the primary and secondary flows. From the experiments carried out in Theistareykir using a rudimentary ejector subsequent modeling of the subsonic ejector by Andal in 2023, a large difference between the primary well and the secondary well made the ejector unable to create sufficient under-pressure and very low secondary mass flow entrainment was observed [3]. Supersonic ejector are more suited for higher pressure differences while subsonic ones could work for lower pressure differences.

The performance of ejectors can be measured in several ways. Some of the key

performance indicators are the entrainment ratio, gained pressure and change in useful energy. The entrainment ratio is the ratio between the secondary and primary mass flow, gained pressure refers to the difference between the outlet pressure and the secondary pressure while the change in useful energy refers to the exergy difference between the exergy at the outlet of the ejector and the exergy at the inlet [3] (See Chapter 4).

The objectives of this study was to use an analytical model developed by Andal [3] to design and then to fabricate a laboratory scale supersonic ejector, carry out experiments to assess its performance with different constant area mixing sections and compare the experimental results to the results from the analytical model. The model was also used to design a potential supersonic ejector to connect two wells in the Olkaria geothermal field in Kenya.

Chapter 2

Background

Ejectors have been used in various applications in the oil and gas [4] and refrigeration [5] sectors. In the geothermal power generation industry, ejectors are widely used to extract non-condensable gases from the condenser. Studies have shown that the use of ejectors to remove non-condensable gases from steam condensers improve their performance. Strusnik et al [6] illustrates the use of ejectors and pumps for gas extraction from steam power plant turbine condensers to improve their heat transfer capabilities and improve process efficiency.

2.1 Ejector principle

Ejectors consist of inlets for the primary and secondary fluids, a nozzle, suction chamber, mixing section and a diffuser. Figure 1 shows a typical supersonic ejector profile and its parts. High pressure or primary fluid accelerates through the nozzle throat and creates low pressure at the nozzle exit. This low pressure allows the secondary fluid to be entrained by suction into the mixing chamber. Mixing of the flows occurs followed by pressure recovery in the diffuser region when the mixture is decelerated further. The kinetic energy of the fluid is then transformed into a pressure rise at the diffuser exit.

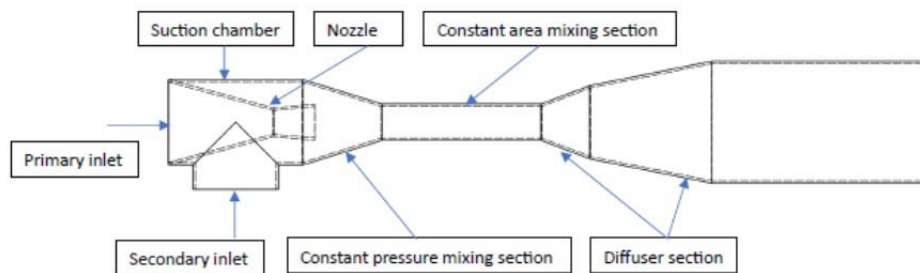


Figure 1: Typical ejector profile and parts [3]

2.2 Classification of ejectors

Ejectors can be classified in various ways. Subsonic and supersonic ejectors are classified depending on the velocity that the primary fluid is accelerated to as it flows through the nozzle. In subsonic ejectors, the flow is accelerated to values below the velocity of sound, while supersonic ones operate at velocities higher than the speed of sound.

Huang et al [7] categorize ejectors as either constant pressure mixing or constant area

mixing depending on the position of the nozzle. According to Chen et al, the constant pressure mixing ejector performs better and is more efficient and is therefore more widely used [8].

Huang et al. [9] describes the functioning of ejectors in three modes: critical mode, sub-critical mode, and back-flow mode. The entrainment ratio ω refers to the ratio between the secondary and the primary mass flow, the back pressure P_c is the pressure at the outlet of the ejector and the critical back pressure P_c^* is the highest back pressure where there is no condition change in mass flow through the ejector.

- (i) *Critical mode* – back pressure, P_c is less than the critical back pressure, P_c^* and both the primary and entrained flows choke (double choking). The entrainment ratio, ω is constant.
- (ii) *Sub-critical mode* – critical back pressure, P_c^* is less than the secondary pressure and secondary pressure is less than the back pressure, P_c . Only the primary pressure is choked (single choking) and entrainment ratio varies with the back pressure.
- (iii) *Back-flow mode* – back pressure is greater than secondary pressure. Both primary and secondary flows do not choke, and the entrained flow is reversed. The entrainment ratio, ω is less than zero and the ejector is said to have malfunctioned.

Figure 2 shows ejector operation modes with respect to pressure and entrainment ratio.

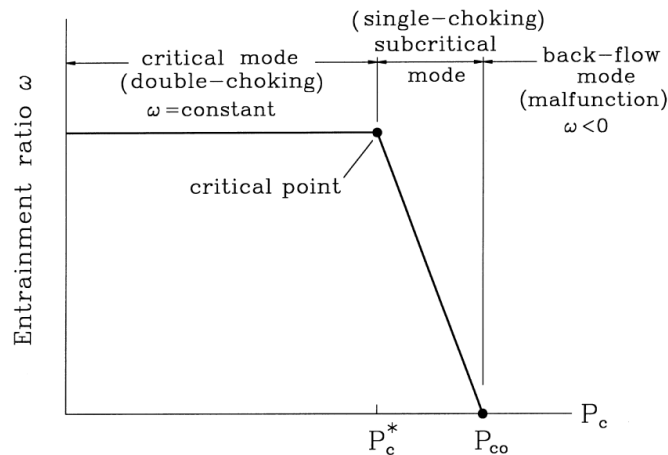


Figure 2: Ejector operation modes with respect to pressure and entrainment ratio [9]

2.3 Industrial uses of ejectors

Most of the applications of the ejector principle in industry are found in the refrigeration industry, oil and gas and geothermal power plants.

2.3.1 Ejector use in refrigeration

Manoj and Lijo [5] describe the basic functioning of an ejector refrigeration system (ERS). The refrigerant vapor is expanded through a nozzle creating a low pressure that initiates the boiling of a secondary fluid from the evaporator and lowers its temperature. The colder secondary fluid can then be used for refrigeration in a secondary circuit. High vapor pressure is created in the evaporator using thermal energy. The reduction in pressure at the ejector allows mixing of the high-pressure fluid from the generator and the lower pressure fluid from the evaporator, leading to the direct use of the colder secondary fluid in the refrigeration process. Figure 3 shows a schematic of the ERS system.

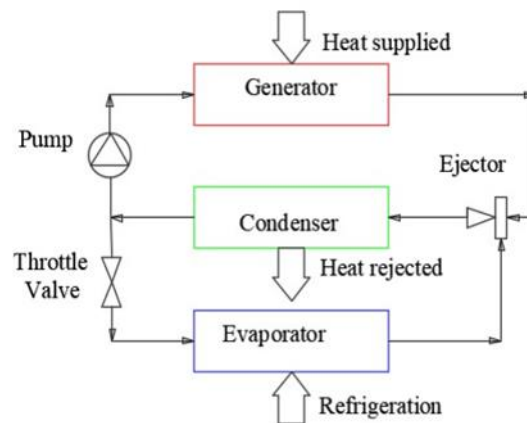


Figure 3: Schematic of ejector refrigeration system [5]

The ejector in the ERS consists of a nozzle and a mixing section. The mixing section is made up of a convergent section, a constant area section and a divergent diffuser section. The high-pressure primary fluid is accelerated through the nozzle throat reaching supersonic speeds at the nozzle exit. This creates a low pressure that allows the secondary flow to entrain, and the two streams fully mix within the constant area section. A normal shock wave within the constant area section creates a compression effect that reduces the velocity to a subsonic value and further velocity reduction occurs in the diffuser section accompanied by a pressure recovery. Figure 4 shows an ejector used in the ERS system.

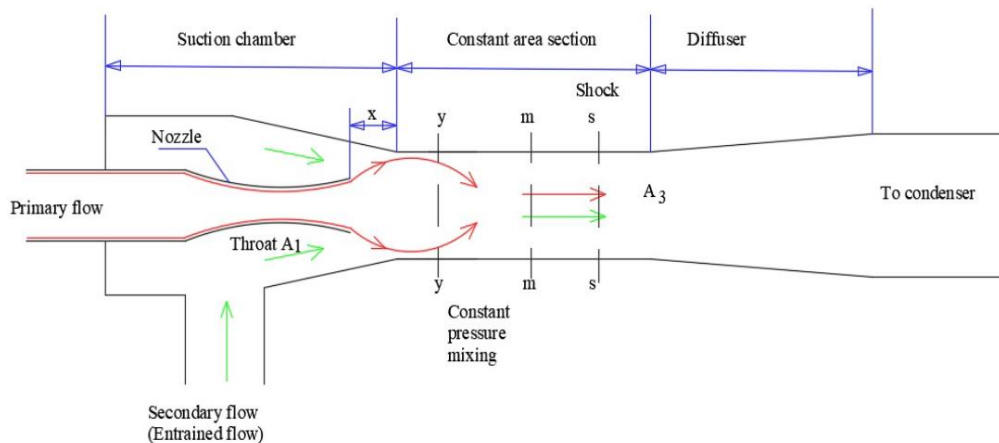


Figure 4: Profile of ejector for ERS [5]

2.3.2 Ejector use in steam power plant condensers

Ejectors in power plants are used to extract non-condensable gases (NCG) from the condenser. Studies show that even a small amount of NCGs drastically impacts the condenser heat transfer potential and power plant output. For single-flash geothermal power plants, the net output and overall exergy efficiency are reduced by 2.7% for every 1% increase in NCG content. [10] because the gases increase the condenser pressure and that decreases the pressure drop through the turbine. Efficient gas extraction is therefore important to ensure any increase in the gas content from the steam does not affect the power output.

Gas extraction in steam power condensers can be done using a steam ejector pump system (SEPS). Figure 5 shows gas extraction system for turbine condensers using SEPS.

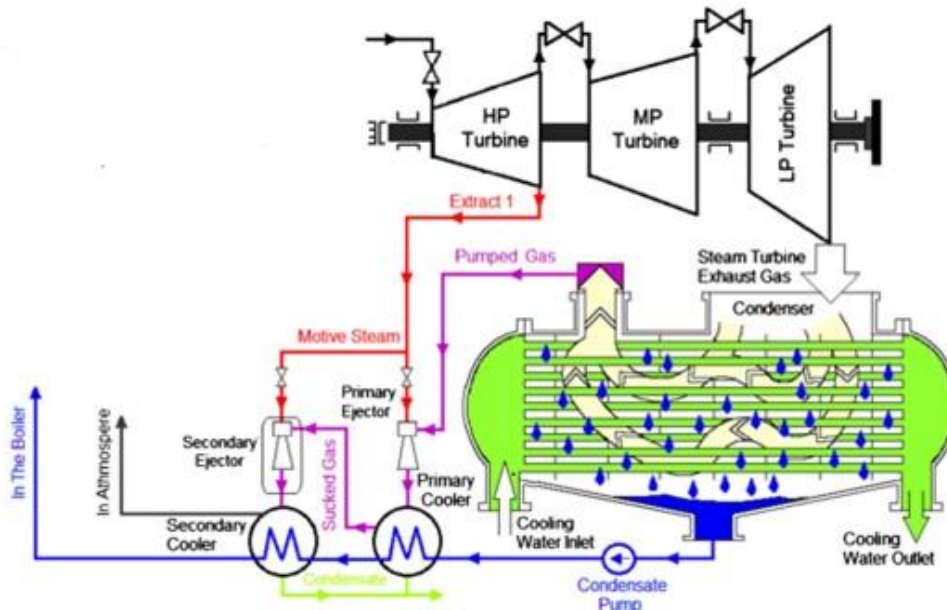


Figure 5: Gas extraction system for turbine condensers using SEPS [6]

This is a two-stage process where NCG is pumped from the condenser and compressed to a pressure of about 0.01MPa. A mixture of this gas and motive steam is fed into a primary cooler where most of the gas condenses. The remaining gas is pumped at steam pressure to a second stage to a pressure slightly higher than atmospheric, then led using motive steam to a secondary cooler. The condensate goes through condensate pots in the condenser, and the residual NCG is released into the atmosphere [6]. The gases can also be reinjected back into the formation.

2.3.3 Ejector use in oil and gas

Pump ejector systems are used in the oil and gas industry to inject petroleum gas when carrying out simultaneous water and gas injection to improve oil recovery from depleted reservoirs. Water alternated gas (WAG) injection and simultaneous water alternated gas (SWAG) injection methods were developed in 1957 and 1962 respectively in Canada and USA to enhance oil recovery as reported by Gorelkina E. [11]. The systems use ejectors to mix water and the associated gases before injection into the reservoir. Associated petroleum gas (APG) is mixed with water and reinjected into oil wells to pressurize wells and increase oil production lifetime. Figure 6 shows a schematic of APG utilization using a pump and ejector. The ejector is used to mix the gas and water before reinjection.

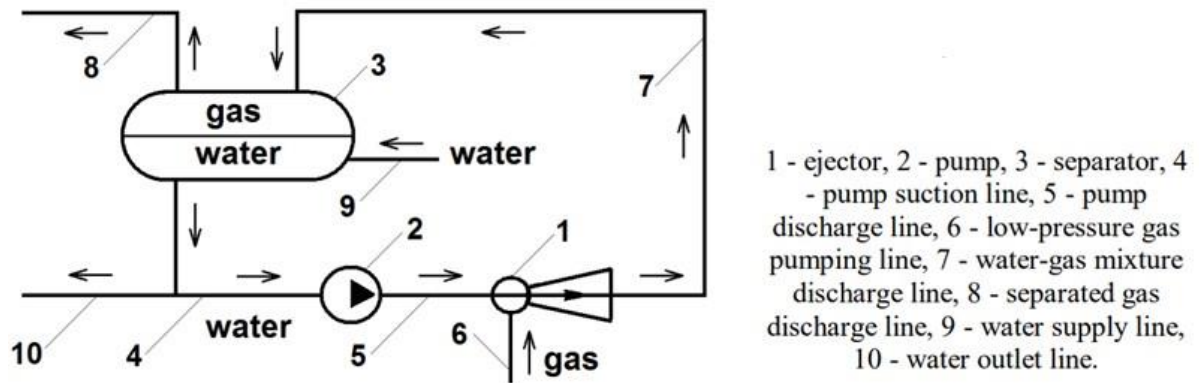


Figure 6: Schematic of APG utilization using a pump and ejector [11]

2.4 Experimental use of ejectors in geothermal wells

Attempts to use ejectors for wells in the geothermal industry were done in a field experiment undertaken in the Theistareykir geothermal field in 2020 and 2021. In the experiment, a rudimentary ejector (Figure 7) was used to connect two wells, ThG-11, which is a high-pressure well and ThG-15, which is a low-pressure, low-enthalpy well using a basic ejector design [12] [13]. The experimental goal was to identify operation conditions that would allow sufficient entrainment of fluid from the low-pressure well using under pressure induced by the high-pressure flow.

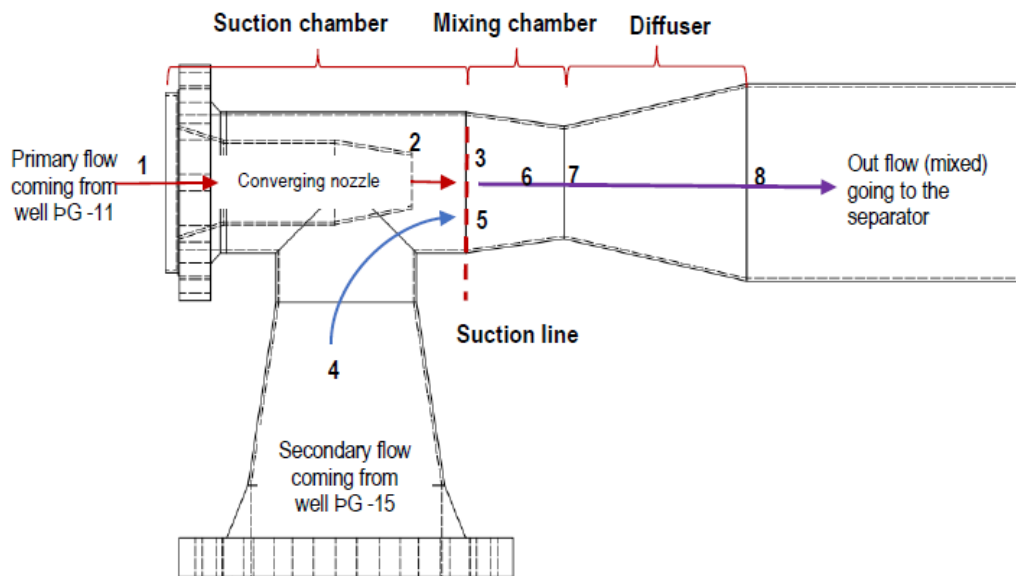


Figure 7: Profile of subsonic ejector for wells ThG-11 and ThG-15 in Theistareykir [3]

Results from the test indicated that this ejector operated within the subsonic region did not provide sufficient induced pressure at the nozzle exit. At some conditions, there was secondary flow entrainment, but the pressure was not able to reach the required level to be connected to the steam gathering system.

Preliminary CFD simulations also suggested that the under-pressure was created further downstream at the throat of the mixing chamber due to further primary flow

acceleration. The absence of a constant area mixing section also meant that there wasn't proper mixing of the primary and secondary flows, which provided challenges in prediction using an analytical model. It was concluded that the design and set-up of the rudimentary ejector could meaningfully entrain the secondary flow, and a supersonic ejector with a convergent-divergent nozzle could be considered.

From the limitations observed on Theistareykir subsonic ejector experiment, Andal developed an analytical model for a supersonic ejector based on the same conditions [3]. A convergent-divergent nozzle and a constant area mixing section were added to improve the performance of the subsonic ejector from the field experiments. The supersonic ejector designed from this work showed that a minimum secondary pressure is required to keep the back pressure and the pressure inside the mixing chamber within the defined constraints. Additionally, the use of ejectors can increase the productivity of wells ThG-11 and ThG-15 by 25 - 40%. The use of ejectors can also be a useful tool in mitigating the effects of silica scaling due to the mixing of the fluid from different wells that would enhance dilution. Figure 8 shows the pressure and velocity profiles from the proposed supersonic ejector developed by Andal in 2023.

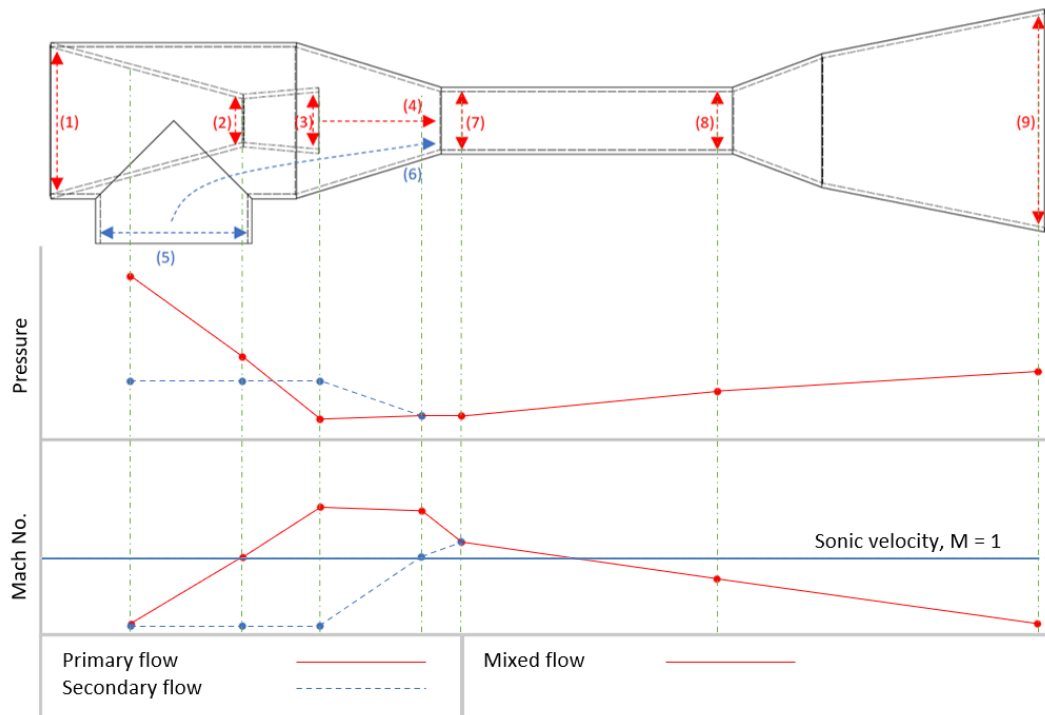


Figure 8: Pressure and velocity profiles for a new proposed supersonic ejector [3]

2.5 Computational fluid dynamics analysis for ejectors

Computational fluid dynamics (CFD) has been extensively used in the analysis of ejector performance. More recently, powerful, and robust tools have been developed like ANSYS Fluent that use finite volume techniques, that are based on discretization of governing equations, by dividing the physical geometry into smaller elements, forming a control volume mesh. Fluid flow through an ejector is unsteady in the 3-D space due to its turbulent nature. The Reynolds-averaged Navier–Stokes (RANS) equations are used for determining averaged values of flow quantities by time averaging over long intervals and

the problem is assumed to be steady and axisymmetric, providing an acceptable level of accuracy.

Huang B. et al [7] pioneered the use of models to predict ejector behavior and performance using a 1-D model. The study analyses the performance of ejectors by defining coefficients that account for losses in the ejector. The coefficients were used to compare analytical and experimental data. The coefficients for losses in the primary and secondary flow η_p and η_s were found to be 0.95 and 0.85, respectively. These coefficients describe deviation from an isentropic process and calculate the inefficiency of conversion to kinetic energy due to entropy generation. The coefficient for the primary flow at nozzle exit ϕ_m was found to vary slightly with the ejector area ratio. The coefficient can be estimated using Equation 1.

$$\phi_m = 1.037 - 0.02857 \frac{A_{CAMS}}{A_t} \quad (1)$$

Where A_{CAMS} is the constant area mixing section area and A_t is the nozzle throat area.

Simulations using CFD by Varga et al, [14] for a supersonic ejector system in the refrigeration industry outlined three key geometrical parameters that are crucial in the performance of ejectors; area ratio between nozzle and constant area mixing section, nozzle exit position (NXP), and constant area mixing section length. Results have shown that increasing the area ratio increases the entrainment ratio, Studies by Rusly et al [15] and Pianthong et al [16] showed that NXP had very minimal effects on the entrainment ratio but concluded that an NXP of 1.5 times the diameter of the constant area mixing section improved the entrainment ratio. The study by Pianthong et al. further observed that a longer constant area mixing section allowed the ejector to be operated in a wider range of conditions.

Chapter 3

Methodology

This work is carried out by comparing experimental results with an analytical model from the work done by Andal in 2023 [3] based on experiments by Huang et al [7] and Chen et al [8]. The experiments use a laboratory scale model of a supersonic ejector sized using the analytical model. Two boilers are then used to simulate the high-pressure and low-pressure streams and pressure and flow rate is measured. The performance of the laboratory sized ejector is then compared to results from the analytical model. The model is also used to design a field-size ejector for selected wells in the Olkaria geothermal field in Kenya.

3.1 Analytical model for a supersonic ejector

The analytical model for the supersonic ejector was developed by Andal in 2023 by improving the subsonic ejector analytical model which was developed earlier from the experiments from Theistareykir geothermal wells (see Section 2.4). The model is adopted was adopted for this. The model code was written using MATLAB with formulae adopted from Chen et al, 2017 and has inbuilt Coolprop functions to calculate the properties of steam and water [17]. Figure 9 shows a supersonic ejector profile with reference points.

The following assumptions and modifications are made to simplify the model.

1. Both primary and secondary flow are assumed to obey the ideal gas laws.
2. The values for constant ratio of specific heat, coefficient of friction and mixing losses and isentropic efficiencies of the nozzle and the entrained flow are adopted from the results of the Theistareykir subsonic ejector performance results as described by Andal, 2023.
 - i. constant ratio of specific heat (C_p/C_v), $k = 1.327$;
 - ii. coefficient of frictional and mixing losses, $c_l = 0.94$; (0.84 originally but 0.94 fitted the experimental results better)
 - iii. isentropic efficiencies of the nozzle and entrained flow, $\eta_n = 0.90$.
3. Mixing of the primary flow and the entrained secondary flow only takes place from the constant area mixing section (from Point 7 on Figure 9), At this point the mixing occurs at constant pressure equal to secondary pressure at this point.
4. Choking of the entrained flow occurs at the hypothetical throat.
5. The model does not account for heat loss through the walls of the ejector.

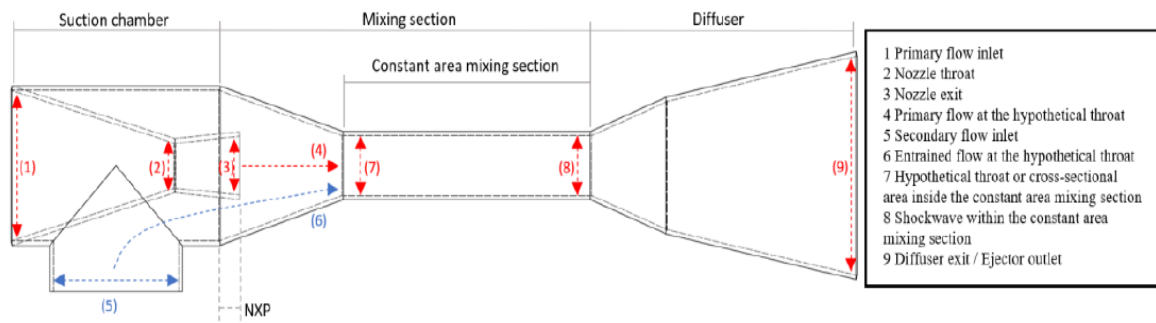


Figure 9: Profile of supersonic ejector [12]

Referring to Figure 9, primary flow is accelerated through the convergent-divergent nozzle and reaches sonic conditions at the nozzle throat (point 2) and supersonic conditions between the nozzle exit (point 3) and constant area mixing section entrance (point 7). This causes a pressure drop in the suction chamber that allows the lower pressure secondary flow to entrain. For model simplification, it is assumed that no mixing takes place until the entrance to the constant area mixing section (point 7). The mixture then undergoes a series of shockwaves within the constant area mixing section and the kinetic energy of the fluid is converted to pressure leading to a pressure recovery in the diffuser section towards the outlet [12]. Figure 10 shows the analytical model process flow chart.

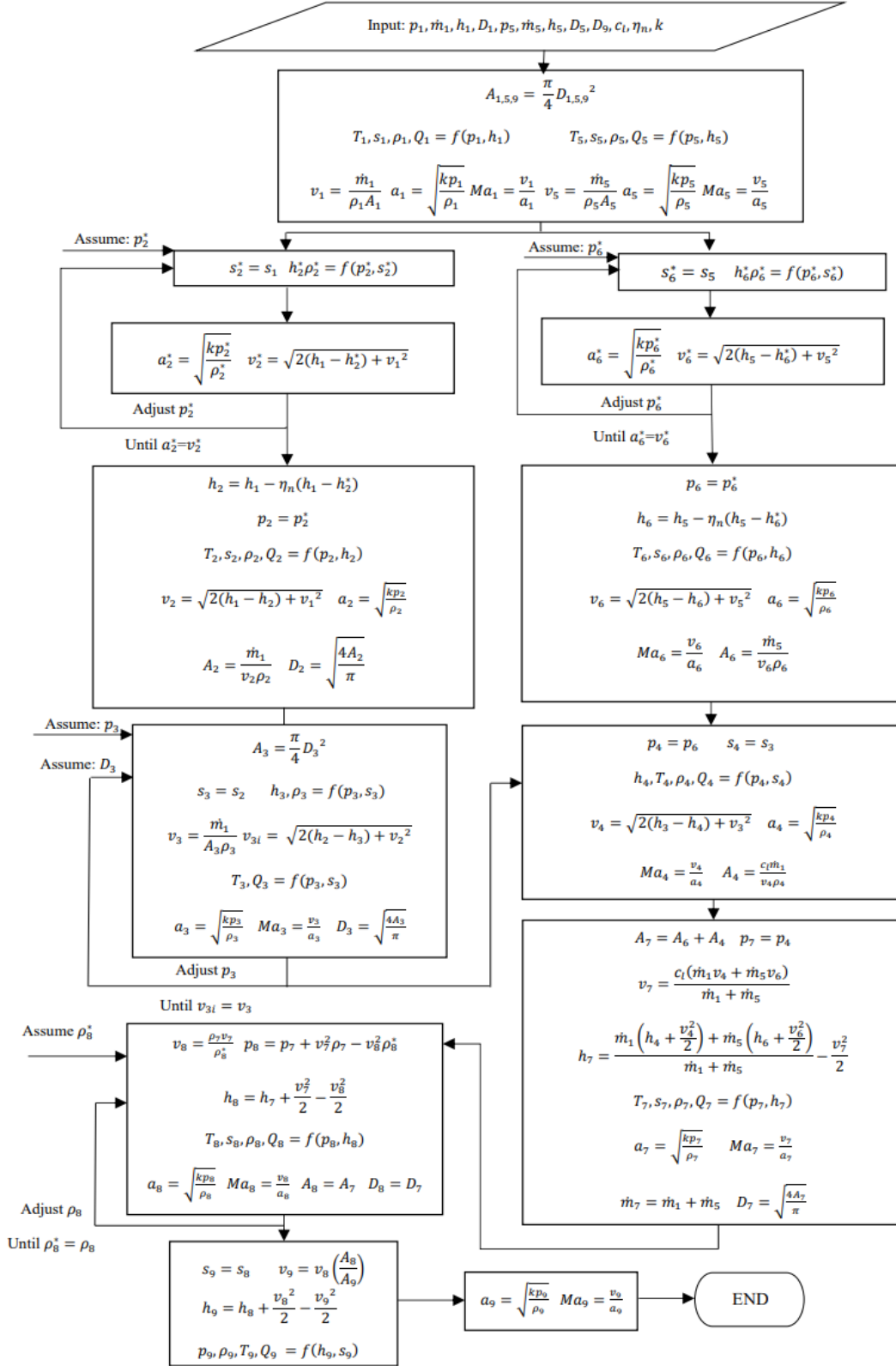


Figure 10: Supersonic ejector analytical model flow chart

Referring to Figure 10, the primary inlet, secondary inlet, and the outlet diameters are predetermined. Input parameters to the model are the pressure, enthalpy, and mass flow for the primary and secondary flows. The nozzle outlet diameter is assumed and by a series of iterations, the calculates the pressure and the enthalpy at the outlet and the diameters of the nozzle throat (Point 2 in Figure 9) and the hypothetical throat (Point 7 in Figure 9). The model should cater for the relationship between the wellhead pressure and the mass flow rate because the mass flow rate though the ejector is limited by the calculated diameters for Point 2 and Point 7 (choke points) even if the well output changes. The model then predicts the performance of the ejector by calculating the pressure, enthalpy and outlet pressure and entrainment ratio with changing primary and secondary conditions and the calculated dimensions for the nozzle throat and hypothetical throat dimensions [3]. The governing equations can be seen on Appendix A.

3.2 Laboratory experiments

Laboratory experiments for this study were carried out in the Reykjavik University energy laboratory. It involved sizing the ejector using the model described in Section 3.1, fabrication of the ejector, assembly of the experimental set-up, carrying out the experiment, data collection and analysis.

3.2.1 Ejector sizing and fabrication

The analytical model from section 3.1 was used to design a laboratory scale supersonic ejector that was used for the experiments. Initial tests were carried out with the primary boiler intended to be used for the high-pressure stream to determine the possible operating conditions. Mass flow, pressure and enthalpy from the initial tests were then used as inputs for the analytical code. Dimensions for the primary inlet, secondary inlet, and the outlet were also predetermined. The code was then used to calculate the dimensions for the nozzle throat, nozzle exit and the constant area mixing section.

Literature from earlier studies have shown that the constant area mixing section (CAMS) affects the performance of supersonic ejectors. Small CAMS tend to increase the pressure in the suction chamber and limit entrainment of secondary flow. Larger CAMS on the other hand create a uniform pressure backwards into the suction chamber and this also limits entrainment of the secondary flow. From the analytical model sizing code, the CAMS diameter of 4.1 mm was predicted. The minimum CAMS diameter was set at 4 mm because of the possible tolerances for local fabrication in the university workshop and the limitations of fabricating an ejector with a smaller CAMS. The analytical model performance code was then used to check the ejector performance as the CAMS diameter was increased. By getting lower entrainment for 4 mm and 9 mm CAMS ejectors, the two sizes were selected as the lower and upper limit and two additional sizes, 5 mm and 7 mm were selected in between by increasing the diameter by 1 mm and 2 mm respectively.

The ejector nozzle was 3D printed from aluminium, and the ejector bodies were fabricated in the university workshop. Processes used include machining, boring and welding. The ejector was then used in four constant area mixing sections (CAMS) of 4 mm, 5 mm, 7 mm, and 9 mm as shown on Figure 11. Summary of the ejector dimensions is shown on Table 1.

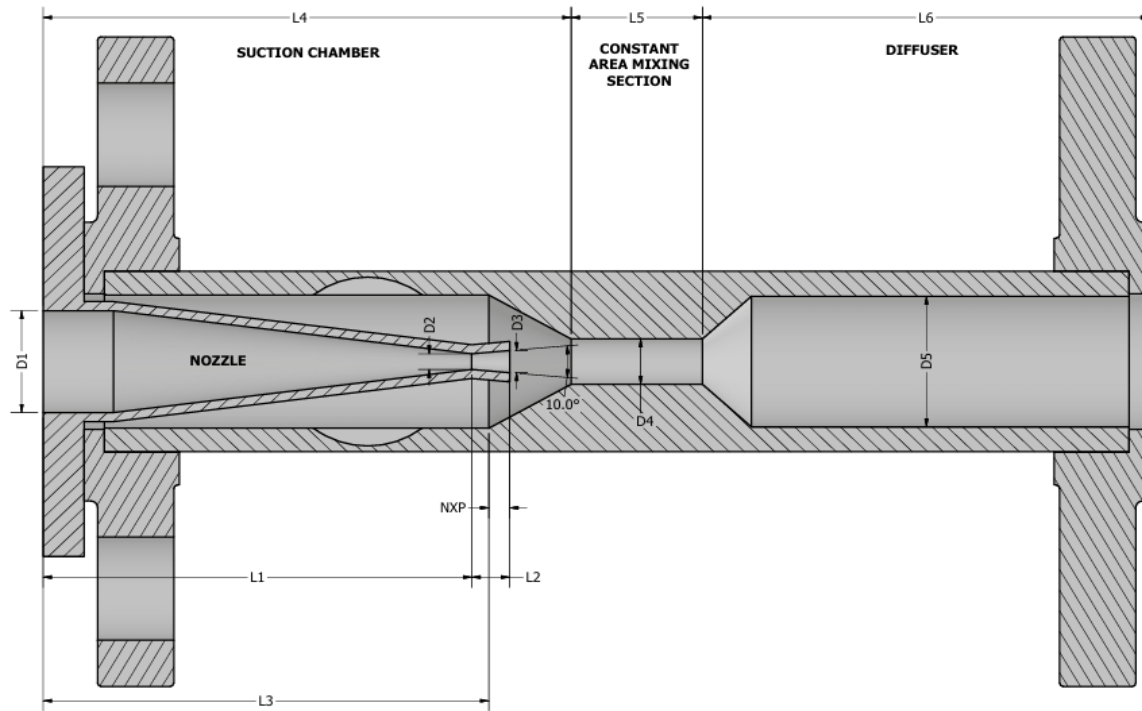


Figure 11: Supersonic ejector dimensions

Table 1: Dimensions for 4, 5, 7 and 9 mm CAMS ejectors used in the experiment

Ejector type	D1 (mm)	D2 (mm)	D3 (mm)	D4 (mm)	D5 (mm)	L1 (mm)	L2 (mm)	L3 (mm)	L4 (mm)	L5 (mm)	L6 (mm)	NXP (mm)
4 mm CAMS	15.7	2.44	3.41	4	20	63	5.57	63.2	74.9	20.9	66.5	5.37
5 mm CAMS	15.7	2.44	3.41	5	20	63	5.57	60.8	75.2	21.2	66.2	7.77
7 mm CAMS	15.7	2.44	3.41	7	20.1	63	5.57	65.5	77.6	19.3	65.7	3.07
9 mm CAMS	15.7	2.44	3.41	9	19.8	63	5.57	64	76.2	19.6	66.7	4.57

3.2.2 Laboratory experimental set-up

The experiment was carried out for each CAMS ejector (see Table 1) with identical procedure and the same inlet conditions to ensure that the data obtained is comparable. Figure 12 and Figure 13 show a pictorial representation of the experiment set-up and the experiment flow schematic respectively.

The operating conditions for the primary flow were selected based on the characteristics of the primary boiler. The primary boiler delivered 0.005 kg/s of steam at an average pressure and temperature of 7.2 bar-g and 212°C. The secondary pressure was set by adjusting the secondary boiler temperature to give a pressure that corresponds to a pressure below the outlet pressure and above the suction chamber pressure as predicted by the analytical model using only the primary flow. This gave a temperature of 169.7°C at a pressure of 2 bar-g.

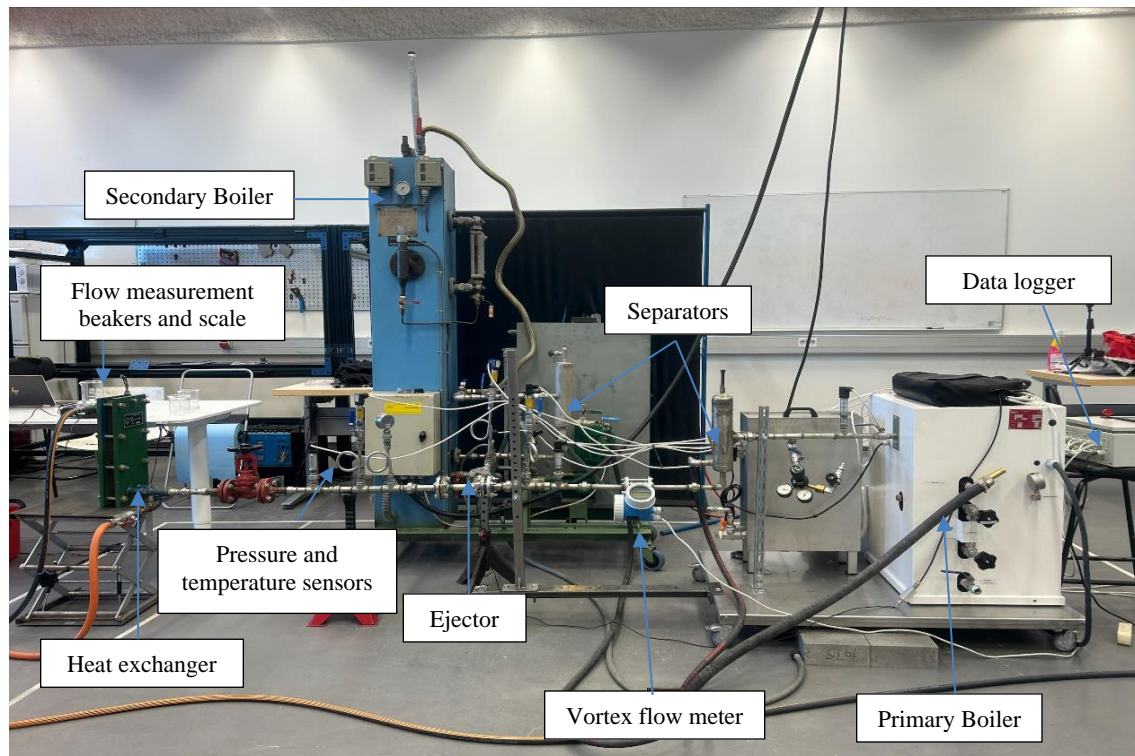


Figure 12: Experiment set-up at Reykjavik University energy laboratory

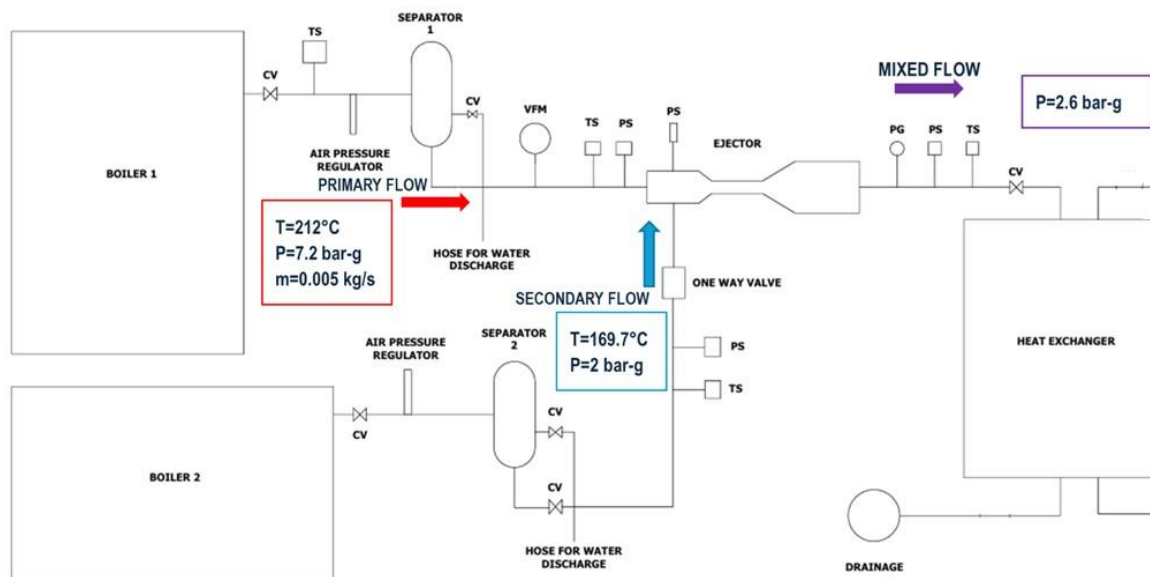


Figure 13: Flow diagram for the experiment

Note: CV – control valve, PS – pressure sensor, TS – temperature sensor, PG – pressure gauge, VFM – vortex flow meter

3.2.3 Equipment used in the experiment

After sizing the ejector using the analytical model sizing code and fabrication, equipment was assembled as shown on Figure 13. The experiment was done to test the performance of the ejector by applying the sizing dimensions selected by the analytical

model. The fabricated ejector was assembled between two boilers that were used to simulate a high-pressure and a low pressure geothermal well respectively. Pressure and temperature sensors were placed on the primary flow path, secondary flow path and the outlet of the ejector (see Figure 13). Separators were assembled at the outlet of the primary and secondary boilers to remove condensation before the ejector. Primary flow measurement was done using a vortex flow meter while secondary mass flow was measured using a beaker and scale from a heat exchanger placed after the ejector outlet. Outlet pressure was set using a valve placed at the outlet and monitored by an online pressure gauge (see experiment procedure in Section 3.2.4). The secondary mass flow was then determined as the difference between the measured mass flow at the outlet when the flows are combined and the measured mass flow of the primary flow only. The specifications of the equipment used are summarized below.

1. Boilers

Two boilers were used to mimic the high-pressure (primary) well and low-pressure (secondary) well. The primary boiler has a 22 kW power rating with a working pressure of 7.2 bar-g and maximum theoretical mass flow of 0.007 kg/s. The secondary boiler has a 24 kW rating with a maximum working pressure of 10 bar-g at a temperature of 175°C. Figure 14 shows pictures of the primary and secondary boilers.

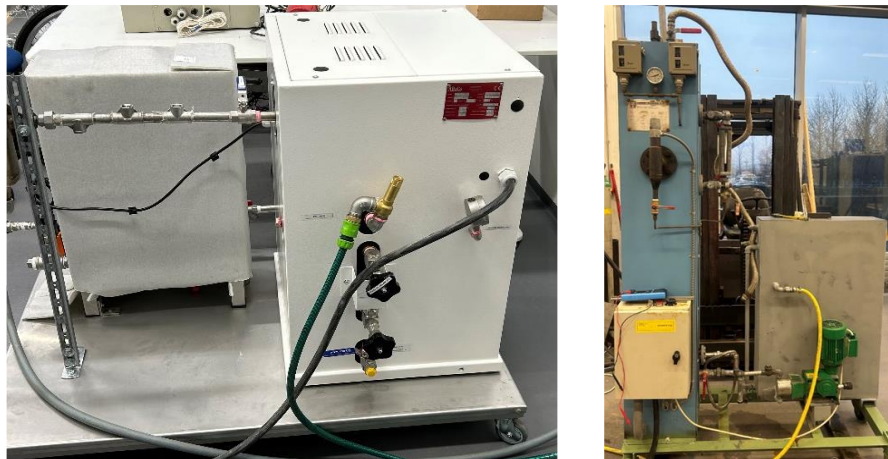


Figure 14: Experiment boilers primary (left) and secondary (right)

2. Steam separators

Steam separator were placed between the boilers and the ejector to remove condensate from the flow and ensure only dry steam reaches the ejector. Miniature vertical cyclone separators were used. The steam separators used are shown in Figure 15.



Figure 15: Experiment steam separators primary (left) and secondary (right)

3. Heat exchanger

A plate type, counter-flow heat exchanger (Figure 16) was used to condense the exit steam and allow for easy mass flow measurement using beakers and a weigh scale. This was also done to verify the accuracy of the vortex flow meter for primary mass flow measurement.

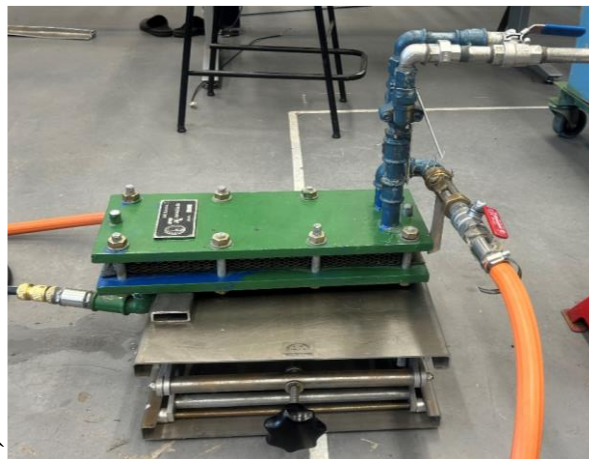







Figure 16: Experiment heat exchanger

4. Measurement devices

Referring to Figure 13, pressure and temperature measurements were carried out using sensors placed in the primary flow path, secondary flow path and the ejector outlet. Data was collected from these sensors during the experiments using a data logger. Outlet pressure (back pressure) was set using a control valve (CV at ejector outlet in Figure 13) and monitored using a pressure gauge placed after the ejector outlet (PG at ejector outlet in Figure 13). Primary flow measurement was done using a vortex flow meter (VFM in Figure 13) and combined flow was measured using a beaker, weigh scale and timer at the heat exchanger outlet. The measurement devices used in the experiment are shown on Table 2.

Table 2: Measurement devices used in the experiment

Device	Quantity	Picture	Specifications
Pressure sensors	3		PCE-28/EXD type Standard ½" thread Accuracy: $\pm 0,2\%$.
Micro pressure sensor	1		JC91 type Pressure: 0.7-10 bar-a Work media: wet/sat steam Temperature: 100-120 °C Mounting : F3=M5x0.8male Thread diameter: 5 mm Thread length: 5 mm Output: A1= 4-20 mA
Pressure gauge	1		Bourdon gauge , 0-12 bar-g SS316 body Glycerine damping
Temperature sensor	4		STA 206 P type mA converter attached. Accuracy: $\pm 0.2^{\circ}\text{C} \pm 0.05 \%$ 30 mm probe.
Vortex flow meter	1		Model: Endress D 200 : Process Temperature: Standard (-40+260°C) Housing: DN15, ½" ANSI Measuring range: 2 to 8342 m ³ /h Working pressure: 10 bar-a Accuracy: $\pm 1\%$ of reading (gases and steam)

Experimental procedure

The following steps describe the procedure that was followed while carrying out the experiment. This procedure was repeated for all the CAMS sizes.

1. The ejector with the nozzle was positioned in place and fastened using bolts and nuts on the flanges.
2. Air pressure was introduced to inspect for leakages and all leaking areas were sealed.

3. The desired output temperature was set corresponding to a pressure of 2 bar-g on the secondary boiler. The primary boiler was to be operated at its maximum working pressure of 7.2 bar-g and a temperature of 212°C.
4. The boiler water tanks were filled.
5. The primary boiler was started, and data recording PLC switched on.
6. The cooling water flow to the heat exchanger was opened.
7. The primary separator water outlet was closed when it was observed that only steam was coming out (separator 1 on Figure 13).
8. When the primary boiler got to its maximum pressure of 7.2 bar-g, the outlet valve was closed to set a backpressure of 2.6 bar-g (above secondary pressure)
9. After waiting for 5 minutes to allow the flow to stabilize, physical measurements of primary flow started at the outlet of the heat exchanger, by taking 12 consecutive mass flow measurement using a beaker, timer, and weigh scale. Physical measurements were taken to verify the accuracy of the readings from the vortex flow meter.
10. Both boiler water tanks were refilled.
11. The secondary boiler was turned on.
12. The secondary separator water outlet was closed when it was observed that only steam was coming out. (separator 2 on Figure 13)
13. After 5 minutes, physical measurement of the combined flow was started at the outlet of the heat exchanger, by taking 12 consecutive mass flow measurement using a beaker, timer, and weigh scale. This was done to compare with the primary mass flow and confirm if there is additional mass from secondary entrainment.
14. The boiler was turned off and PLC recording also stopped.
15. The separator water and outlet valves were opened to depressurize and cool the system.
16. After cooling, the ejector was removed and replaced with the next CAMS ejector.
17. The logged data was then downloaded for analysis. The logged data was pressure data from the primary, secondary, outlet and suction chamber pressure sensors, temperature data for the primary, secondary and outlet temperature sensors and mass flow data from the vortex flow meter. Additional mass flow data from physical measurements of primary flow and combined flow were also analyzed.
18. This process was replicated for all the four CAMS sizes.

Chapter 4

Results

4.1 Laboratory experiment results

From the experiments with the four different constant area mixing sections (CAMS), the results are plotted for pressure, temperature, and mass flow over the duration of the experiments. The pressure measurements are plotted for primary flow, secondary flow, suction chamber, and the outlet. The temperature measurements are plotted for primary flow, secondary flow, and flow at the outlet. The mass flow measurements are plotted for primary mass flow from the vortex flow meter and the combined flow at the outlet as measured using beakers, a weigh scale, and a timer at the outlet of the heat exchanger (see Figure 13).

From the pressure profiles, primary flow pressure remains stable and constant during the experiment. The wavy pattern for the primary flow is due to resetting of the boiler that is automatic as a safety mechanism. The outlet pressure also remains constant but rises most significantly for the 5 mm CAMS ejector when the secondary flow is introduced. The suction chamber pressure is above the secondary pressure for the 4 mm but stays almost equal to or slightly below the secondary pressure for the rest of the CAMS ejectors.

The temperature profiles shows a similar pattern with the primary and outlet temperature remaining constant and the temperature flow increasing at the secondary temperature sensor locations after the introduction of secondary flow. A rise in the outlet temperature after introducing secondary flow could denote entrainment. The 4 mm, 7 mm, and 9 mm CAMS ejectors showed a lower difference between the outlet temperature with primary flow only and the temperature with combined flow.

The primary mass flow was measured using the vortex flow meter as steam flow and verified by outlet measurements after condensation using beakers, weigh scale and a timer at the outlet of the heat exchanger (see Figure 13). The error in the two measurements methods was only 4% and this confirmed their accuracy.

Experimental results for the 4 mm CAMS ejector are shown in Figure 17.

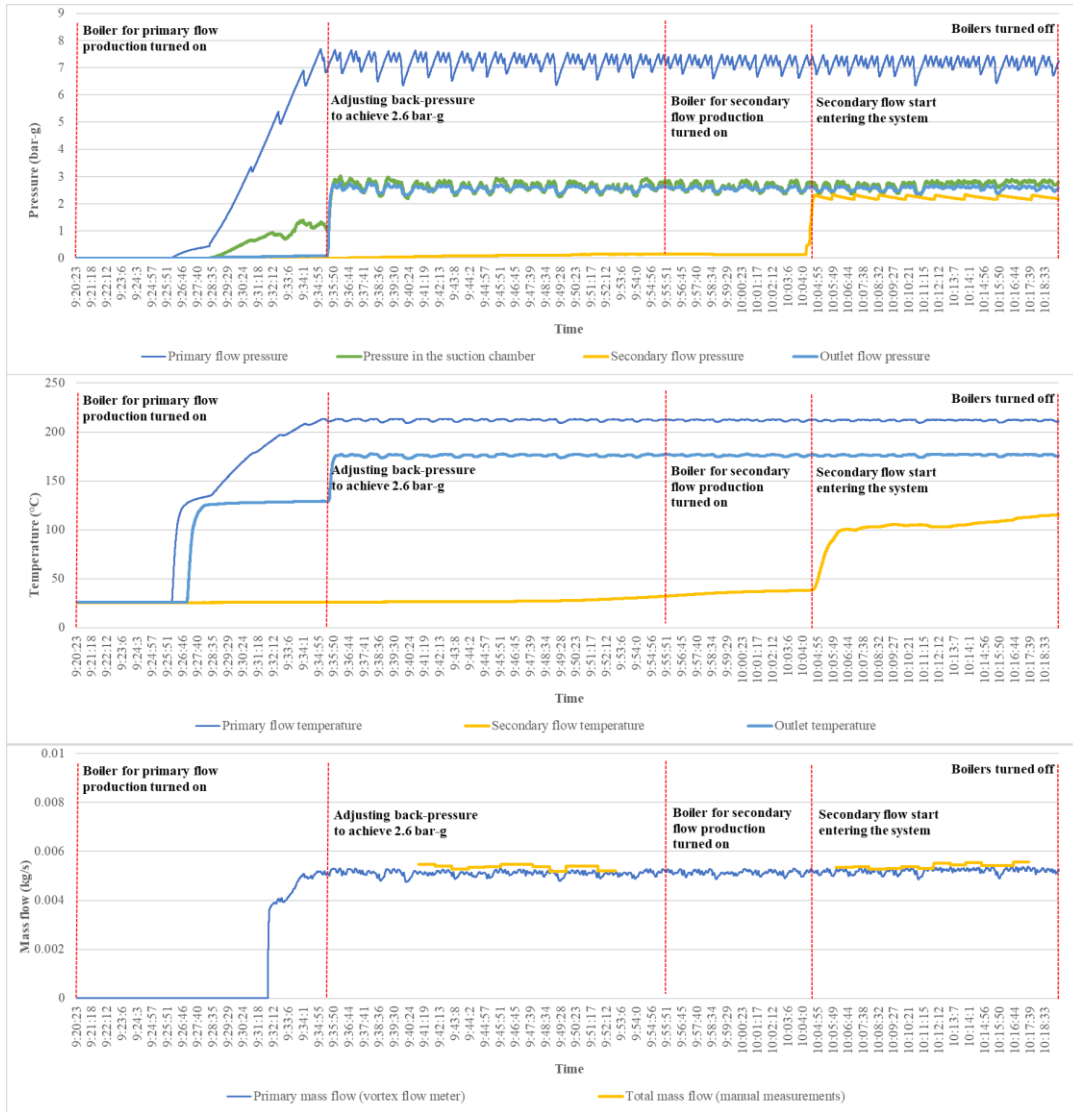


Figure 17: Experimental results for 4 mm CAMS ejector Pressure (top), Temperature (middle) and Mass flow (bottom)

Referring to Figure 17 (top), the 4 mm CAMS ejector showed almost equal suction chamber and outlet pressure. The secondary pressure was however observed to be lower than the suction chamber pressure after introduction of the secondary flow. There is also no significant change in the outlet mass flow as can be seen in Figure 17 (bottom).

The results from the 5 mm CAMS ejector can be seen in Figure 18

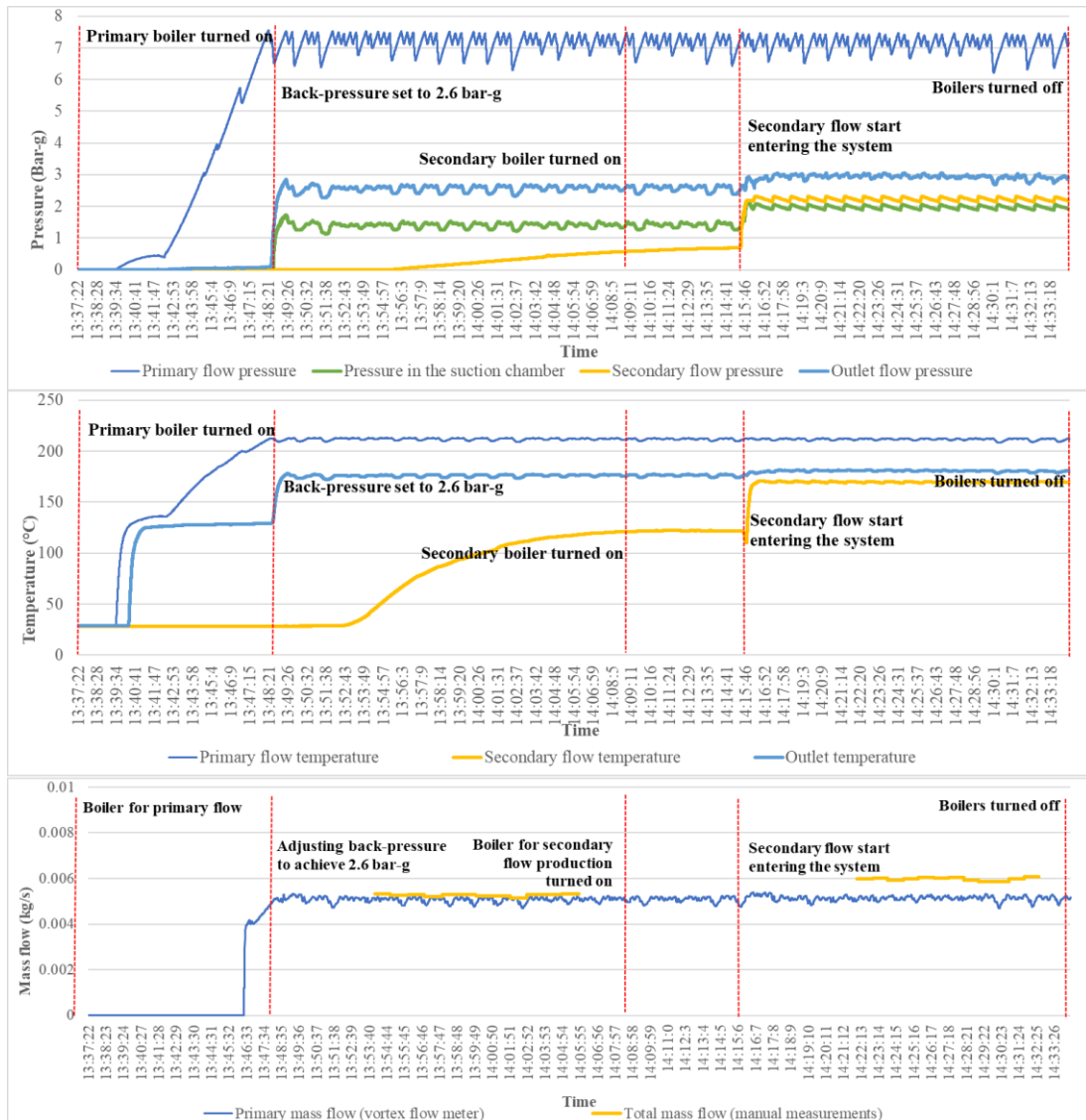


Figure 18: Experimental results for 5 mm CAMS ejector Pressure (top), Temperature (middle) and Mass flow (bottom)

The results of pressure from the 5 mm CAMS ejector (Figure 18, top) show a significant increase in the outlet pressure after introduction of the secondary flow. There is also an increased suction chamber pressure, but the secondary flow pressure remains above the suction chamber pressure. This creates secondary mass flow into the ejector resulting to entrainment as can be seen in Figure 18, bottom.

Figure 19 shows the results from the 7 mm CAMS ejector.

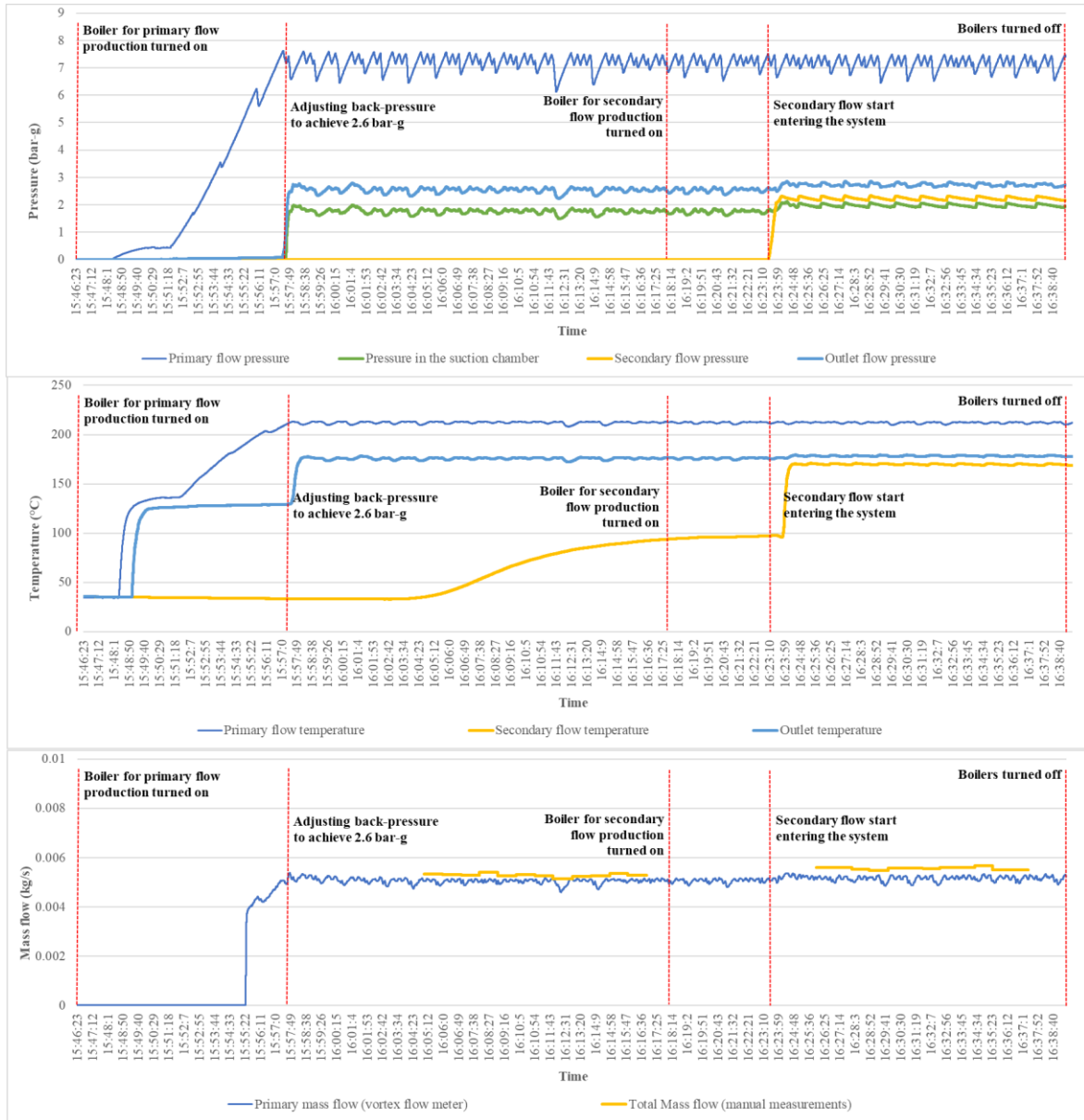


Figure 19: Experimental results for 7 mm CAMS ejector Pressure (top), Temperature (middle) and Mass flow (bottom)

For the 7 mm CAMS ejector (Figure 19), results like the 5 mm CAMS ejector are seen but with a slightly lower difference between the secondary pressure and the suction chamber pressure. The additional mass flow at the outlet is however lower than that of the 5 mm CAMS ejector.

The results from the 9 mm CAMS ejector can be seen in Figure 20.

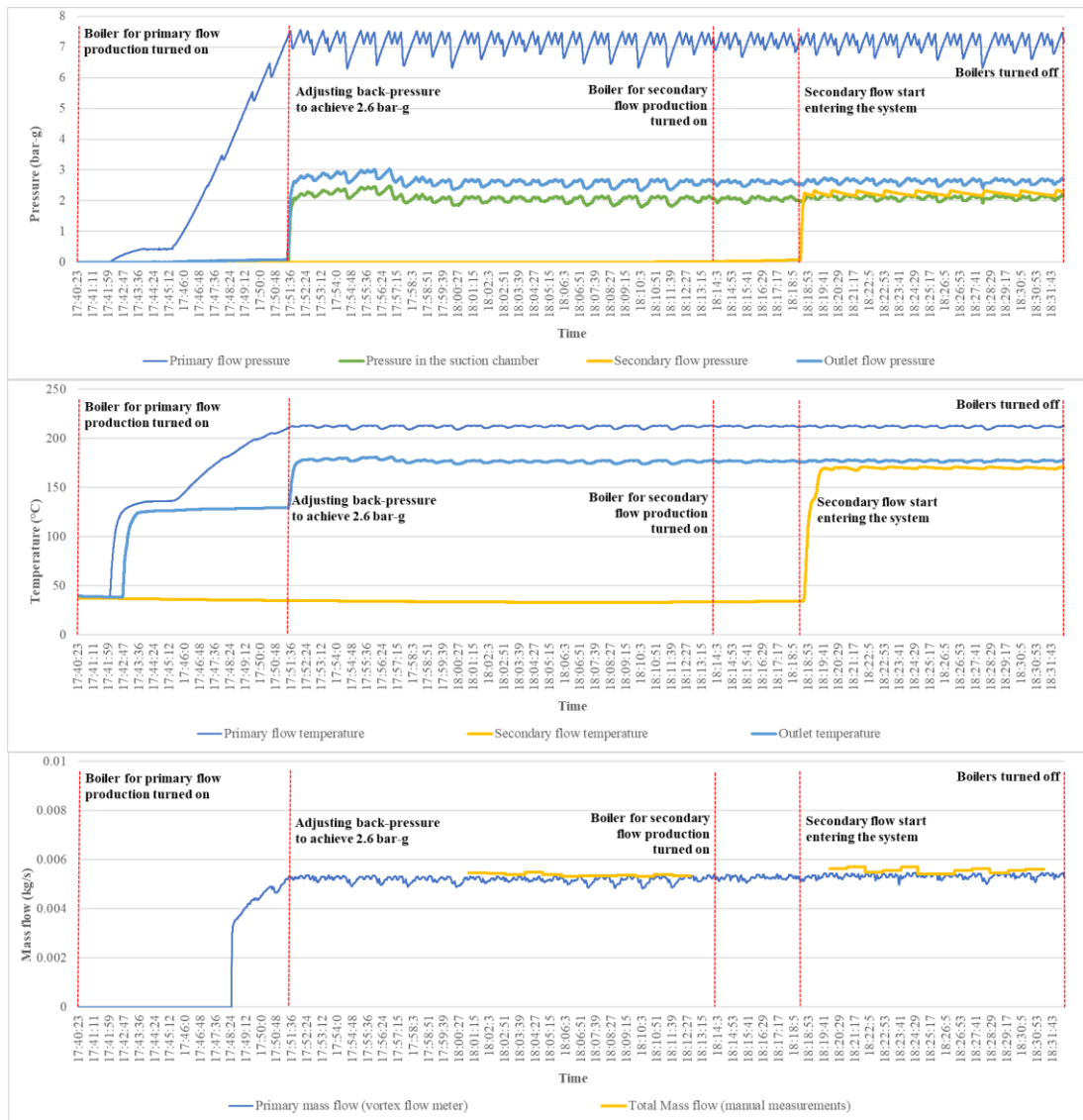


Figure 20: Experimental results for 9 mm CAMS ejector Pressure (top), Temperature (middle) and Mass flow (bottom)

The 9 mm CAMS ejector results show a similar trend to the 4 mm CAMS ejector as shown on Figure 20. The suction chamber and secondary pressures are very similar and there is an insignificant difference between the measured primary and the outlet mass flows.

The performance of the four CAMS ejectors was carried out using the gained pressure, entrainment ratio and an exergy analysis as performance indicators (see Chapter 1). The effects of the area ratio on their performance was also analyzed.

4.1.1 Gained pressure

Gained pressure (see Equation 2) is defined as the difference between the outlet pressure P_o and the secondary pressure P_s . This is the additional pressure gained by the introduction of secondary flow through the ejector.

$$\text{Gained pressure} = P_o - P_s \quad (2)$$

P_o and P_s represent outlet and secondary pressure respectively. (in Figure 13, P_o is

measured by the PS at the ejector outlet and P_s is measured by the PS on the secondary flow line before the one-way valve).

From the collected experimental data, the gained pressure was calculated by considering the combined average outlet flow pressure recorded by the pressure sensor at the outlet of the ejector after stable conditions were achieved and the average secondary flow pressure, also recorded by the pressure sensor at the secondary inlet after attaining stable conditions. Table 3 shows a summary of the average values of measured pressure for the primary flow, secondary flow, suction chamber pressure, flow at the outlet, and the calculated gained pressure from the experimental data.

Table 3: Summary of pressure results from the experiment

CAMS diameter (mm)	Average primary pressure (bar-g)	Average secondary pressure (bar-g)	Average suction chamber pressure (bar-g)	Average outlet pressure (bar-g)	Gained pressure (bar-g)
4	7.15	2.23	2.70	2.57	0.34
5	7.12	2.23	1.97	2.94	0.71
7	7.16	2.23	1.97	2.73	0.50
9	7.14	2.34	2.10	2.63	0.39

From Table 3, the average values of primary and secondary pressure remained very similar for all the CAMS size ejectors. The 5 mm and 7 mm CAMS ejectors showed similar values for suction chamber pressure. The 5 mm showed the highest gained and outlet pressure.

4.1.2 Entrainment ratio

Entrainment ratio, ER refers to the ratio between the secondary mass flow \dot{m}_s and the primary mass flow \dot{m}_p as shown in Equation 3.

$$ER = \frac{\dot{m}_s}{\dot{m}_p} \quad (3)$$

Where, \dot{m}_s and \dot{m}_p represent the secondary and primary mass flow respectively.

Primary mass flow data was obtained using the vortex flow meter and verified by physical measurements using beakers and a weigh scale. The mass flow at the outlet for combined flow was done using the beakers and weigh scale only. The secondary flow was then calculated as the difference between the average combined flow and the average primary flow, and the entrainment ratio calculated using Equation 3. Table 4 shows a summary of the calculated entrainment ratio from the experimental data.

Table 4: Entrainment ratio results from the experiment

CAMS diameter (mm)	Entrainment ratio, ER
4	0.038
5	0.166
7	0.081
9	0.041

From Table 4, the results show that the entrainment ration and the gained pressure show a similar trend with the 5 mm CAMS ejector showing the highest entrainment ratio.

4.1.3 Area ratio effects

Earlier studies from Varga et al [14] identified area ratio, AR which is the ratio between the nozzle and the constant area mixing section as one of the critical geometrical parameters affecting the performance of supersonic ejectors. Area ratio is described by Equation 4.

$$AR = \frac{A_{CAMS}}{A_t} \quad (4)$$

Where, A_{CAMS} is the area of the constant area mixing section and A_t is the area of the nozzle throat.

From Table 1, all the ejectors used a common nozzle of throat diameter 2.44 mm. The effects of the varying area ratio on gained pressure, entrainment ratio and suction chamber pressure were assessed. Table 5 and Figures 21 and 22 show the experimental results.

Table 5: Area ratio effects from the experiment

Nozzle throat diameter (mm)	CAMS diameter (mm)	Area ratio, AR	Gained pressure (bar-g)	Entrainment ratio, ER
2.44	4	2.69	0.339	0.038
2.44	5	4.20	0.708	0.166
2.44	7	8.23	0.498	0.081
2.22	9	13.61	0.394	0.041

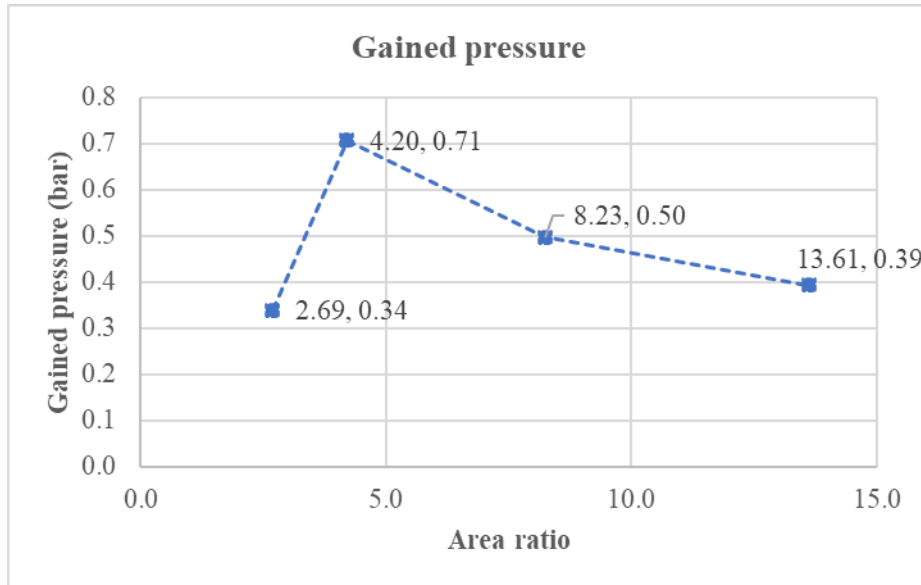


Figure 21: Effect of area ratio on gained pressure

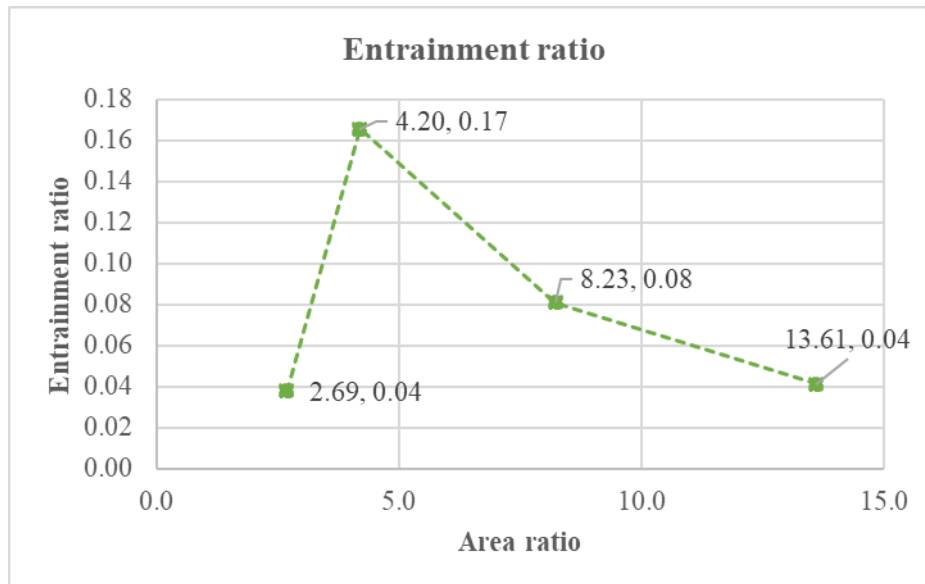


Figure 22: Effect of area ratio on entrainment ratio

From Figures 21 and 22, the 4.2 area ratio for the 5 mm CAMS ejector showed the highest gained pressure and entrainment ratio.

4.1.4 Exergy analysis

An exergy analysis was done to establish the useful work gained from the ejector. This would then determine the amount of additional energy that can be obtained at the outlet of the ejector for conversion to electrical or thermal energy from the process if used for geothermal power generation. A simplified exergy analysis was carried out on the 5 mm CAMS ejector by considering only two components, physical exergy and kinetic exergy as shown in Equation 5, 6 and 7.

$$\text{Total specific exergy, } e = (e_{PE} + e_{KE}) \quad (5)$$

$$\text{Specific physical exergy, } e_{PE} = h_k + h_o - T_o(s_k - s_o) \quad (6)$$

$$\text{Specific kinetic exergy, } e_{KE} = \frac{V_k^2}{2} \quad (7)$$

Where \dot{m} is the mass flow rate, h is specific enthalpy, T is the temperature, s is the entropy, V is fluid velocity and subscripts k and o represent the flow and ambient conditions respectively.

Exergy was calculated for the primary flow, secondary flow, and the combined flow at the outlet. Figure 23 shows the results of the exergy analysis.

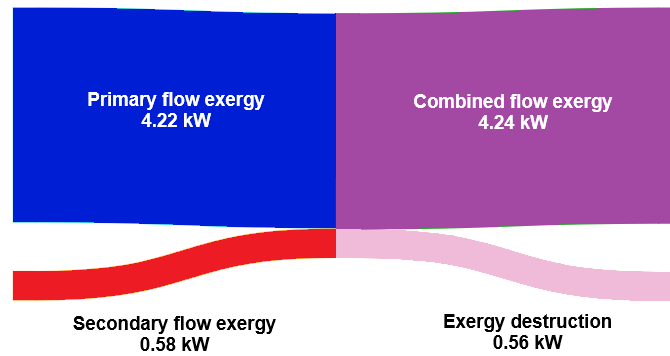


Figure 23: Grassman diagram for 5 mm CAMS ejector

The exergy results show a total exergy from the primary and secondary flows at the inlet of the ejector of 4.8 kW. The outlet exergy is 4.24 kW. This indicates an exergy loss of 0.56 kW and an exergy efficiency of 0.88.

4.2 Comparison of the analytical model and experimental results

After completion of the laboratory experiments and the analysis of the data, the results from the experiments were compared to results from the analytical model to understand the model predictions and account for modifications before using the ejector in designing real size ejectors for geothermal power plants.

The analytical model described in Section 3.1 was used to assess the performance of the ejector using experimental conditions for the four CAMS sizes used in the experiment.

Average value of pressure and enthalpy from the experiment were used as inputs into the performance prediction code. The predicted values for gained pressure, entrainment ratio, outlet (back) pressure and outlet temperature for each of the CAMS used is as shown in Table 6.

4.2.1 Entrainment ratio

Table 6 shows the comparison entrainment ration from the experimental results and the prediction of the analytical model. The model overpredicts the entrainment ratio in all the four cases while the experiment shows almost no entrainment for the 4 mm and 9 mm

CAMS ejectors. The 5 mm CAMS ejector shows the highest entrainment ratio from the experiment, but the 9 mm CAMS ejector shows the highest entrainment ratio for the analytical model.

Table 6: Experiment and analytical model comparison for entrainment ratio

CAMS	Area ratio, AR	Entrainment ratio, ER	
		Analytical model	Experiment
4 mm	2.7	0.55	0.04
5 mm	4.2	1.16	0.16
7 mm	8.2	2.80	0.08
9 mm	13.6	5.04	0.04

4.2.2 Gained pressure

A comparison of the gained pressure from the experiment and the model can be seen on Table 7. There is a good match for the 5 mm CAM ejector. The model, however, shows higher values for the 4 mm CAM ejector and lower value for the 7 mm and 9 mm. (See Table 7.)

Table 7: Experiment and analytical model comparison for gained pressure

CAMS	Area ratio	Gained pressure	
		Analytical model	Experiment
4 mm	2.7	1.23	0.34
5 mm	4.2	0.67	0.71
7 mm	8.2	0.12	0.50
9 mm	13.6	-0.14	0.39

4.2.3 Back or outlet pressure

There is a good correlation between the back pressure measurements from the experimental results and the analytical model results for the 5 mm CAMS ejector as shown on Table 8. The model, however, overpredicts back pressure for the 4 mm CAMS ejector and underpredicts it for both the 7 mm and 9 mm. The lower back pressure predicted by the model explains the higher entrainment from the 7 mm and 9 mm CAMS ejectors.

Table 8: Experiment and analytical model comparison for back pressure

CAMS	Area ratio	Back pressure	
		Analytical model	Experiment
4 mm	2.7	3.56	2.57
5 mm	4.2	2.99	2.94
7 mm	8.2	2.45	2.73
9 mm	13.6	2.20	2.63

Table 9 shows the experimental results and analytical model comparison of the outlet temperature for the 9 mm CAMS ejector. The outlet temperature shows a good match between the experiment and the model for all the CAMS. The model however marginally overpredicts for the 4 mm and 5 mm CAMS ejectors and marginally underpredicts for the 7 mm and 9 mm CAMS ejectors.

Table 9: Experiment and analytical model comparison for outlet temperature

CAMS	Area ratio	Outlet temperature	
		Analytical model	Experiment
4 mm	2.7	193.0	176.4
5 mm	4.2	185.8	180.7
7 mm	8.2	177.9	178.3
9 mm	13.6	172.2	177.1

4.3 Analytical model application for Olkaria wells

The experimental results show that the ejector can be used to entrain flow from a lower pressure well using a high pressure well. This is evident from the under-pressure created in the suction chamber and the additional mass flow measured at the outlet of the ejector. An ejector can therefore potentially be designed to enhance flow from a lower pressure well. There are however limitations due to the wet steam from geothermal wells and more work on the analytical model for two-phase flow and field experiments are required to complete the design of such an ejector.

Olkaria geothermal field in Kenya, like many other geothermal fields, has wells that were drilled and could not be connected due to their pressure being lower than the pressure of the steam gathering system. Additionally, some wells are productive at the beginning of their lives but naturally decline over time as they are used. These wells are sometimes close to high pressure production wells and may be connected using ejector technology and continue being useful for power generation. Using these wells can reduce the requirement for make-up wells and therefore also reduce the total capital costs and improve the power plant output.

An assessment was done for pairs of high-pressure and low-pressure wells that could potentially be connected using a supersonic ejector to make use of the lower pressure wells for power generation using the analytical model. The results showed that wells 905 and 905B were potential candidates for connection using an ejector due to their mass flow, stable wellhead pressure and sufficient outlet pressure when combined.

Well 905 is a high-pressure production well connected to the steam gathering system for a 10 bar-a wellhead plant while well 905B was drilled on the same well pad but could not be connected due to its low-pressure characteristics. Figure 24 shows a map of well pad for wells 905 and 905B.



Figure 24: Map showing wells 905 and 905B on the well pad.

Table 10 shows the flow characteristics of the wells at maximum flow pressure. Flow measurement for well 905 is the latest flow test while that of well 905B is from discharge test data after drilling. The output curves for the wells is shown in Figure 25. The quality of the flow from the wells show that the flow from the wells is wet saturated steam which poses a limitation to the methodology described in this study.

Table 10: Flow characteristics for wells 905 and 905B in Olkaria

Well	Wellhead pressure (bar-a)	Mass flow (kg/s)	Enthalpy (kJ/kg)	Steam quality
905	31.0	33.5	1758	0.53
905B	7.5	14.1	1668	0.63

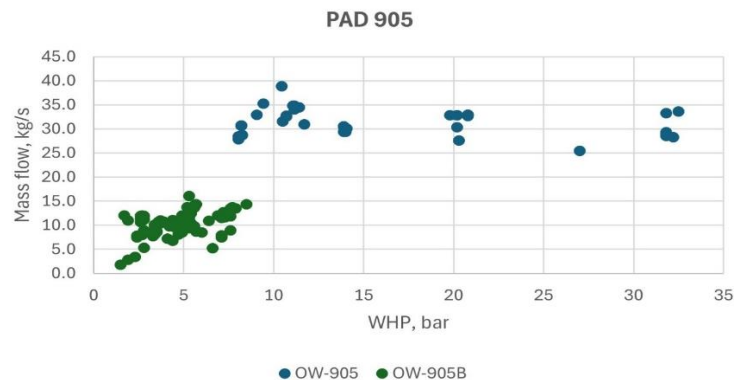


Figure 25: Output curves for wells 905 and 905B

4.4 Analytical model results for Olkaria wells

The analytical model was used to assess the possibility of connecting wells 905 and

905B using the supersonic ejector presented in Section 3.1. The supersonic ejector is preferred because of the large difference between the wellhead pressure of primary well and the secondary well. The analytical model was first used to size the ejector using pressure, mass flow and enthalpy as inputs. Dimensions from the sizing were then used as inputs to assess its performance with the pressure and enthalpy as inputs. A requirement for this model is that the outlet pressure needs to be above the steam gathering system pressure of 10 bar-a (9 bar-g). Using the analytical model, an assumption was made that the flow from the wells is homogenous with mixture properties. Other assumptions made were as in the analytical model (see Section 3.1). The results are shown in Table 11.

Table 11: Analytical model results for wells 905 and 905B

Points	1	2	3	4	5	6	7	8	9
Parameter	Entrance primary flow	Nozzle throat	Nozzle exit	Primary flow at hypothetical throat	Entrance Secondary flow	Secondary flow at hypothetical throat	Mixing chamber	Shock wave	Diffuser exit / Ejector exit
Diameter (cm)	25	8.3	11.7	11.3	25	10.1	15.2	15.2	35
Mass flow, (kg/s)	33.1	33.1	33.1	33.1	11.9	11.9	45.0	45.0	45.0
Pressure (bar-g)	31.5	15.6	3.6	3.4	7.5	3.4	3.4	6.6	9.2
Enthalpy (kJ/kg)	1758	1706	1595	1595	1668	1616	1622	1712	1731
Fluid velocity (m/s)	17.5	322.0	571.6	578.0	47.4	322.4	399.4	239.0	42.7

Figure 26 shows the pressure and velocity profiles for the wells as calculated using the analytical model.

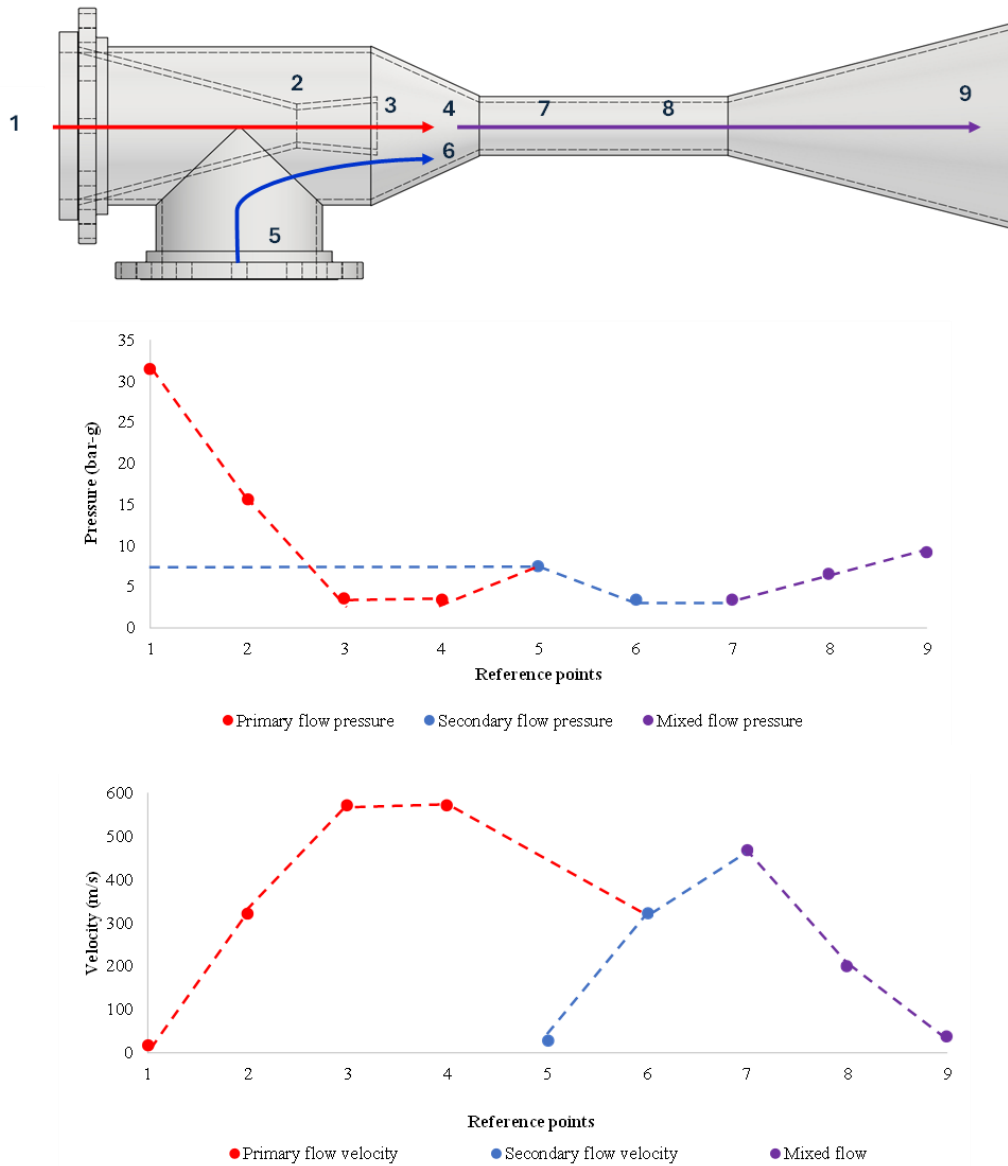


Figure 26: Pressure and velocity profiles for 905 and 905B ejector

4.4.1 Exergy analysis

Exergy analysis was carried out as one of the performance indicators for the ejector designed for wells 905 and 905B in Olkaria. Exergy efficiency was done by considering exergy losses for the flow through the ejector. Figure 27 shows the exergy loss calculations for the flow through the ejector.

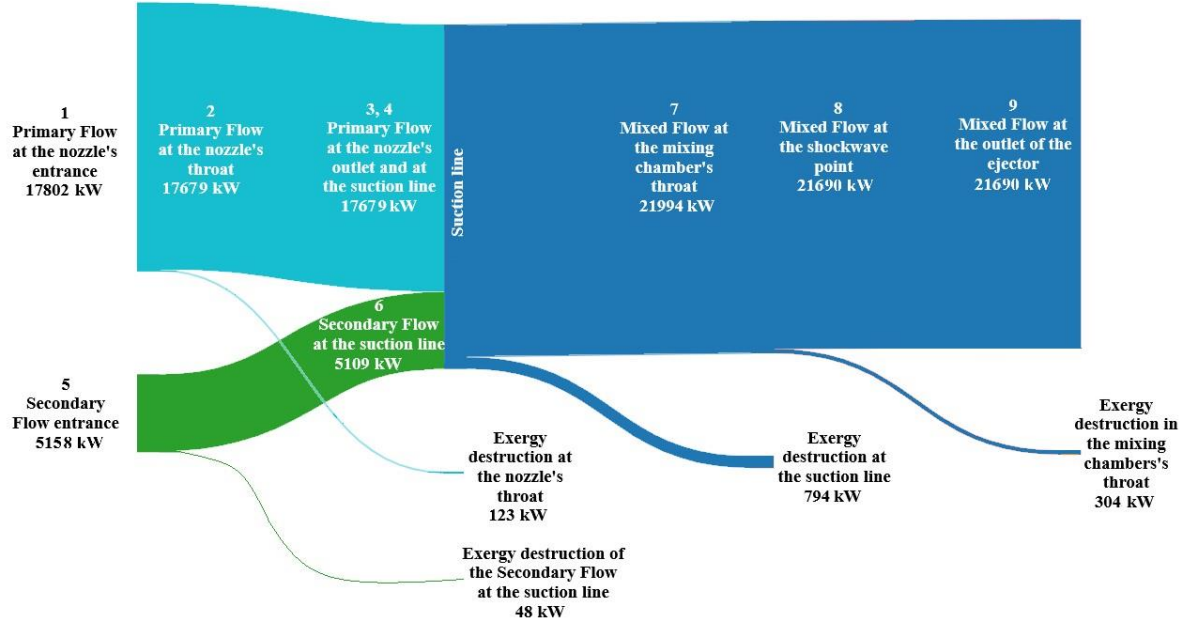


Figure 27: Grassman diagram for wells 905 and 905B in Olkaria connected with an ejector

From the analysis, largest exergy destruction occurs in the suction chamber possibly due to enthalpy reduction caused by mixing of the two streams. The exergy efficiency is calculated using Equation 8.

$$\text{Exergy efficiency, } \eta_{ex} = \frac{e_9}{e_1 + e_5} \quad (8)$$

Where e_9 is the exergy at the outlet of the ejector for the combined flow, and e_1 and e_5 are the exergies for the primary and the secondary flow at the inlets of the ejector.

The highest exergy destruction is in the mixing chamber due to an enthalpy and velocity drop as the secondary and primary streams mix in comparison to the primary flow at the nozzle exit. Minor exergy destruction is observed at the nozzle throat due to the assumed nozzle isentropic efficiency of 0.9 and at the ejector exit due to a reduction in velocity caused by an increase in the flow area. The calculations show an exergy efficiency of 0.94.

Gained pressure is calculated as the additional pressure that the secondary flow attains flowing through the ejector. From Equation 2, the gained pressure is the difference between the outlet pressure and the secondary pressure. The pressure gained by well 905B is calculated as 1.7 bar-g.

The entrainment ratio is used as a performance indicator for the ejector by calculating the ratio between the entrained secondary mass flow and the primary mass flow (see Equation 3). For wells 905 and 905B, the entrainment ratio was calculated as 0.4.

The added is obtained from the difference between the power from the primary wells alone and the power from the combined wells using an ejector. The added power was calculated from the exergy analysis in Section 4.4.1. From Figure 26, primary exergy e_1 is 17.8 MW and the outlet exergy or useful exergy e_9 is 21.6 MW. Using Equation 9, added electrical power is determined.

$$\text{Added electrical power, } MW_e = \frac{(e_9 - e_1)}{1.72} \quad (9)$$

The added power is calculated as 2.2 MW_e. This shows that by using an ejector, the power output is increased by 21% compared to using the primary well only. Table 12 shows a summary of the performance indicators for the ejector design proposed for connecting wells 905 and 905B in the Olkaria geothermal field.

Table 12: Performance indicators for wells 905 and 905B ejector

Gained pressure (bar-g)	1.7
Entrainment ratio	0.4
Added power (MW _e)	2.2
Exergy efficiency	0.94

Chapter 5

Discussion

The experimental results confirm the functioning of the supersonic ejector principle with gained pressure and secondary mass flow entrainment observed for all the four CAMS ejectors used in the experiment.

From the experiment, the highest gained pressure is seen in the 5 mm CAMS ejector and lower values for the 4 mm and 9 mm CAMS ejectors. The gained pressure for the 5 mm CAMS was 0.71 bar-g while that of the 4 mm CAMS ejector was 0.34 bar-g.

The entrainment ratio was also highest for the 5 mm CAMS at 16.6% while the 4 mm and the 9 mm had entrainment ratio below 5%. Low entrainment ratio in the 4 mm and 9 mm CAMS ejectors may be because for the 4 mm CAMS ejector, the small diameter almost acts like a second nozzle and creates a pressure build-up in the suction chamber increasing the suction chamber pressure and affecting entrainment. For the 9 mm CAMS ejector, the increased diameter creates a uniform pressure between the suction chamber and the CAMS, and this would similarly reduce entrainment.

The experimental results show that the ratio between the CAMS and the nozzle throat (area ratio) affects the ejector performance. The optimum area ratio from the experimental results is 4.2 from the 5 mm CAMS ejector.

The comparison of experimental results and the analytical model was done for entrainment ratio, gained pressure, back pressure and outlet temperature. The comparison, however, had limitations because the conditions of the experiment could not be fully replicated in the analytical model and therefore the model could not be validated by the experimental results.

The comparison shows a good match for the outlet pressure and outlet temperature. The gained pressure and the entrainment ratio, however, do not compare well. The entrainment ratio is overpredicted by the model for all the CAMS ejectors because as the CAMS is increased, the ejector tends to act like a pipe and more of the secondary flow goes through and the model calculates the mass flow as flow through a pipe without the ejector effects. The gained pressure is higher in the model than in the experiment for the 4 mm CAMS ejector and lower for the rest. For the 7 mm and 9 mm CAMS ejectors, the analytical model shows no gained pressure and more entrainment than in the experimental results.

The comparison for the back pressure shows a good agreement between the experimental results and the analytical model. It is however important to note that the back pressure is a predicted value in the analytical model but set at a fixed value at the beginning of the experiment. The analytical model predicts slightly lower values than what is seen in the experiments for the 7 mm and 9 mm CAMS ejectors.

The outlet temperature also showed a good match but was slightly underpredicted by the model for the 7 mm and 9 mm CAMS ejectors.

The analytical model used to design an ejector for wells 905 and 905B in Olkaria geothermal field assumed a homogenous fluid with mixture properties from the wells. Additionally, the experiment and model did not show a good match for the entrainment ratio and the gained pressure. The application of the model in designing real size ejectors needs

to be backed up by future work and more experiments. Entrainment ratio and gained pressure may also need to be corrected when using the model for real size designs.

The model shows that by connecting the wells using an ejector, there is a gained pressure of 1.7 bar-g, an entrainment ratio of 0.4 and an exergy efficiency of 0.94. The added electrical power is 2.2 MW when compared to using the high-pressure well only.

Chapter 6

Conclusion and recommendations

6.1 Conclusion

The outlet pressure and the outlet temperature from the experimental results compared well with the analytical model results. The entrainment ratio and the gained pressure, however, did not provide a good match.

The laboratory experiments showed that the 5 mm CAMS ejector had the best performance in terms of the entrainment ratio, gained pressure and the suction chamber pressure. From the experimental results, an area ratio of 4.2 (for the 5 mm CAMS ejector) was considered the optimum.

The ejector designed to connect wells 905 and 905B in Olkaria geothermal field in Kenya showed a gained pressure of 1.7 bar-g and an entrainment ratio of 40%. An additional 2.2 MW of electrical power can be generated if wells 905 and 905B are combined using an ejector than if the high-pressure well is used alone. This represents an electrical power output increase of 21% and an ejector exergy efficiency of 94%.

Despite the results deviating from the analytical model predictions, the experiment was successful because it showed that the ejector principle was working from the gained pressure and entrainment ratio seen in the experimental results.

6.2 Recommendations

The experiment was not able to validate the analytical model. More laboratory and field experimental work is therefore needed to validate the model by trying to get better matches for the gained pressure and entrainment ratio.

The analytical model and the laboratory experiments were based on steam while for the wells in Olkaria, the ejector design was done using two-phase fluid with mixture properties. Further work should focus on the effects of low steam quality on the performance of the ejector.

The analytical model assumes that there is no heat loss through the wall of the ejector. Future experiments should consider insulation of the ejector and connected pipework to try and get better matches between the experiment and the model.

The experiment did not consider the impacts of other ejector geometric parameters like NXP and CAMS length on the ejector performance. These factors should be considered in future experiments to better understand their effects.

Results for the Olkaria wells need to be backed up by experimental field work like the experiments at Theistareykir to provide data that can be used to further improve the analytical model.

Bibliography

- [1] ESMAP, "Geothermal Handbook: Planning and Financing Power Generation," World Bank, Washington DC, 2012.
- [2] Besagni. G., "Ejector on the cutting edge: The past, the present and the perspective," *Energy*, vol. 170, pp. 998-1003, 2019.
- [3] J. M. Andal, "Geoejector: Extracting fluid from a low-pressure geothermal well, MSc thesis report," Reykjavik University, Reykjavik, 2023.
- [4] Andreussi P., Sodini S., Faluomi V., Ciandri P., Ansiati A., Paone F., Battaia C., De Ghetto G, "Multiphase ejector to boost production: First application in the Gulf of Mexico," in *Offshore Technology Conference*, Houston, 2003.
- [5] L. V. Manoj P. J., "Recent developments in ejector refrigeration system," *Materials Science and Engineering*, vol. 1114, 2021.
- [6] Strušnik D., Golob M., Avsec J, "Effects of non-condensable gas on heat transfer in steam turbine condenser and modeling of ejector pump by controlling gas extraction rate through extraction tubes," *Energy Conversion and Management*, vol. 126, pp. 228-246, 2016.
- [7] Huang, B., Chang, J., Wang, C., & Petrenko V, "I-D Analysis of Ejector Performance," *International Journal of Refrigeration*, vol. 22, no. 5, pp. 354-364, 1999.
- [8] Chen, W., Shi, C., Zhang, S., Chen, H., Chong, D., and Yan, J, "Theoretical Analysis of ejector refrigeration system performance under overall modes," *Applied Energy*, vol. 185, pp. 2074-2084, 2017.
- [9] Huang. B. and Chan. J., "Empirical Correlation for Ejector Design," *International Journal of Refrigeration*, vol. 22, no. 5, pp. 379-388, 1999.
- [10] Yildırım Ozcan, N., and Gokcen, G, "Performance analysis of single-flash geothermal power plants, gas removal system point of view," *Geothermal energy technology and geology*, pp. 227-260, 2012.
- [11] Gorelkina E, "Improvement of pump ejector systems in order to increase the gas discharge pressure and system efficiency," *Earth and environmental science*, vol. 6666, no. 6, 2021.
- [12] Andal J., Ragnar Lárusson R., Muguruza G, Sævarsdóttir G., Tesfahunegn Y., Júlíusson E., Sveinsson K, Chauhan V., Guðjónsdóttir M., "Improvement of geoejector design using an analytical model and data from Theistareykir geothermal field," in *World Geothermal Congress*, Beijing, 2023.
- [13] Guardia M., Andal J., Ragnar Lárusson R., Sævarsdóttir G., Tesfahunegn Y., Júlíusson E., Sveinsson K, Chauhan V., Guðjónsdóttir M., "Connecting high and low-pressure geothermal wells using an ejector: Analysis of first field tests at the Theistareykir geothermal power plant," in *World Geothermal Congress*, Beijing, 2023.
- [14] Varga S., Armando C. Oliveira, Bogdan Diaconu B, "Influence of geometrical factors on steam ejector performance - A numerical assessment," *International Journal of Refrigeration*, vol. 32, no. 7, pp. 1694-1701, 2009.
- [15] Rusly E., Aye L, Charters W.W.S., A. Ooi A, "CFD analysis of ejector in a combined ejector cooling system," *International Journal of Refrigeration*, vol. 28, no. 7, pp. 1092-

1101, 2005.

- [16] Pianthong, K., Seehanam, W., Behnia, M., Sriveerakul, T., & Aphornratana., "Investigation and improvement of ejector refrigeration system using computational fluid dynamics technique," *Energy conversion and Management*, vol. 48, no. 9, pp. 2556-2562, 2007.
- [17] Bell, I. H., Quoilin, S., Wronski, J., & Lemort, V., "Coolprop: An open source reference-quality thermophysical property library," in *ASME ORC 2nd International Seminar on ORC Power Systems*, Rotterdam, 2013.

Appendix A Analytical model equations

Figure A1 shows the analytical model for the supersonic ejector and Figure A2 shows the position on the ejector that the process parameter subscripts refer to.

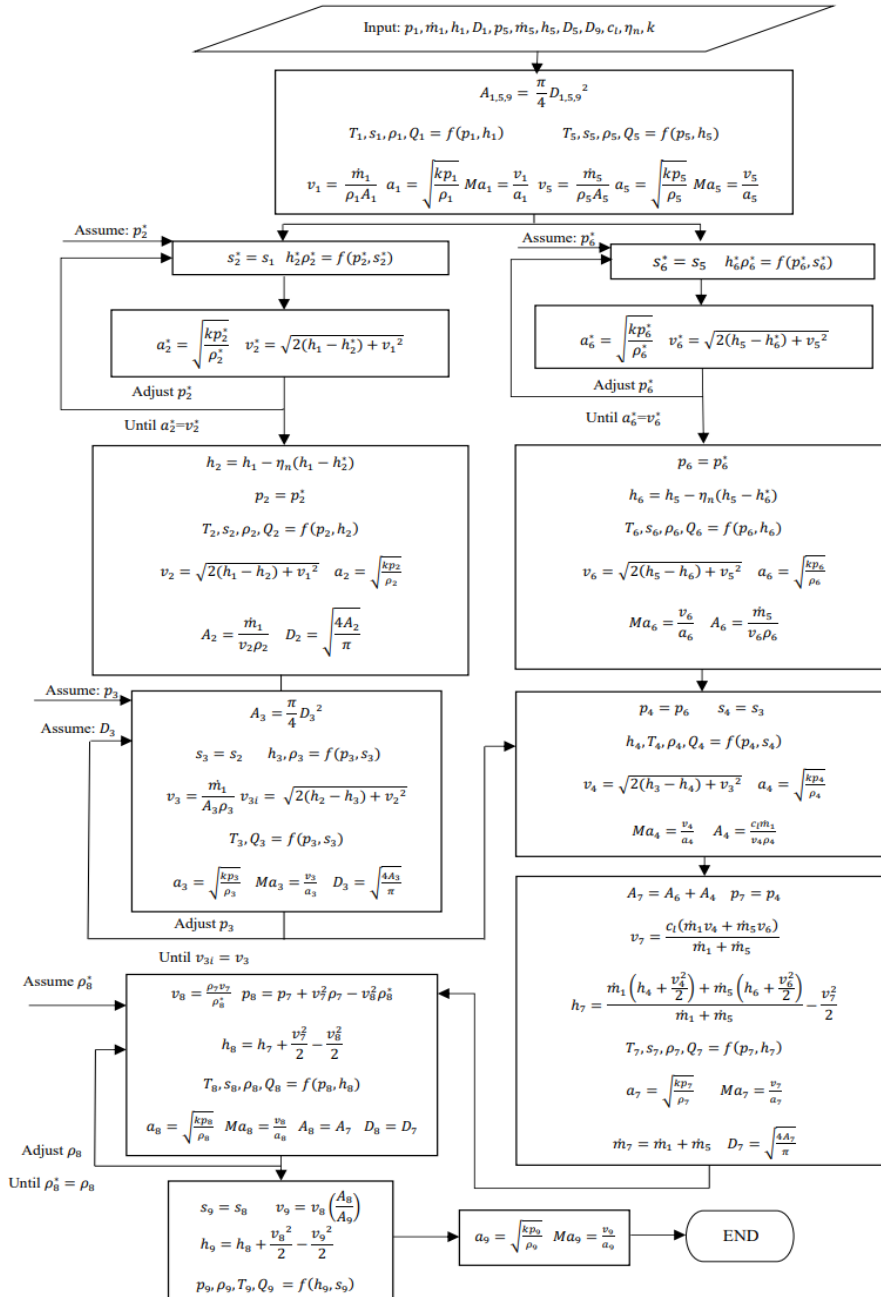


Figure A1: Supersonic ejector analytical model flow chart.

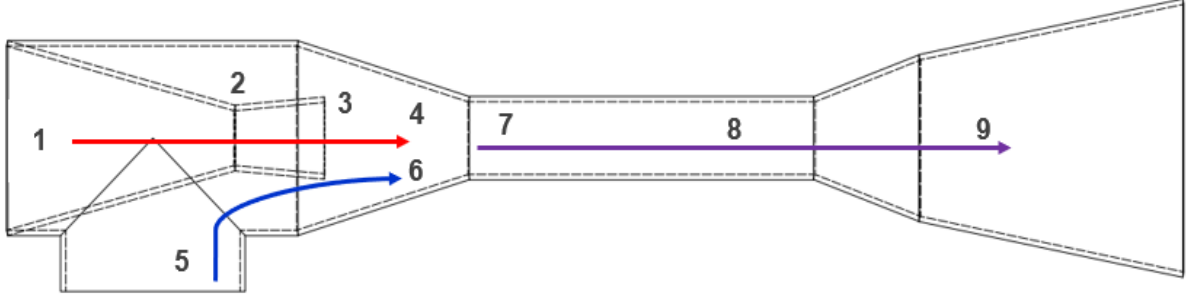


Figure A2: Supersonic ejector profile with subscript reference points.

Primary flow enters the ejector through the primary inlet (Point 1) and gets accelerated to sonic flow through the nozzle throat (Point 2). The pressure and enthalpy at the nozzle throat (p_2 , and h_2) is obtained iterating p_2 until the velocity at the throat reached sonic conditions i.e. $v_2^* = a_2^*$ (Equations A1 and A2). v_1 is the velocity at the primary inlet.

$$v_{2|p_2}^* = \sqrt{2(h_1 - h_{2|p_2}^*) + v_1^2} \quad (\text{A1})$$

$$a_{2|p_2}^* = \sqrt{\frac{kp_2}{\rho_{2|p_2}^*}} \quad (\text{A2})$$

Assuming the compressible flow through the nozzle is isentropic, then enthalpy at the nozzle throat (Point 2) can be calculated from the isentropic enthalpy, h_2^* using Equation A3. η_n is the isentropic efficiency of the nozzle.

$$h_2 = h_1 - \eta_n(h_1 - h_2^*) \quad (\text{A3})$$

Pressure, p_2 , calculated using Equations 1 and 2, and enthalpy, h_2 , from Equation 3 are then used to calculate velocity and density at the nozzle throat. Using these values with the primary mass flow rate, \dot{m}_1 , are the used to calculate nozzle throat area A_2 using Equation A4.

$$A_2 = \frac{\dot{m}_1}{v_2 \rho_2} \quad (\text{A4})$$

At the nozzle exit (Point 3), a value is randomly assigned for the nozzle exit diameter D_3 . The pressure at the nozzle exit, p_3 is then iterated until the two velocity equations (Equations A5 and A6) are equal. D_3 is then optimized to meet all the constraints.

$$v_3 = \frac{\dot{m}_1}{\rho_{3|p_3} A_3} \quad (\text{A5})$$

$$v_3' = \sqrt{2(h_2 - h_{3|p_3}) + v_2^2} \quad (\text{A6})$$

At the hypothetical throat (point 6), secondary flow that has entrained is assumed to reach sonic or choked flow. Pressure, p_6 , and enthalpy, h_6 , of the secondary flow is calculated by iterating the pressure until the fluid velocity, v_6^* , equals to sonic velocity, a_6^* ,

using Equations A7 and A8.

$$v_{6|p6}^* = \sqrt{2(h_5 - h_{6|p6}^*) + v_5^2} \quad (\text{A7})$$

$$a_{6|p6}^* = \sqrt{\frac{kp_6}{\rho_{6|p6}^*}} \quad (\text{A8})$$

Using the isentropic efficiency, η_n , Equation A9 is used to adjust the enthalpy h_6^* for critical conditions.

$$h_6 = h_5 - \eta_n(h_5 - h_6^*) \quad (\text{A9})$$

Using the calculated pressure, p_6 , (Equations 7 and 8) and adjusted enthalpy, h_6 , (Equation A9), velocity and density of the secondary flow before the hypothetical throat is calculated. The values obtained together with the secondary mass flow rate, \dot{m}_5 , are used to determine area of the hypothetical throat occupied by the entrained flow, A_6 using Equation A10.

$$A_6 = \frac{\dot{m}_5}{v_6 \rho_6} \quad (\text{A10})$$

Assuming the two flows start to mix with uniform pressure equal to pressure of the entrained flow and that flow between the nozzle and the hypothetical throat (Point 4) is isentropic, Equation A11 is used to calculate the hypothetical throat area occupied by the primary flow A_4 . c_l is a coefficient introduced to cater for losses.

$$A_4 = \frac{c_l \dot{m}_1}{v_4 \rho_4} \quad (\text{A11})$$

Constant area mixing section (point 7) area A_7 is the sum of the areas occupied by the primary flow and the entrained flow before the hypothetical throat. This is calculated using Equation A12.

$$A_7 = A_6 + A_4 \quad (\text{A12})$$

As the two streams will start to mix inside the constant area mixing section, velocity v_7 can be calculated using a momentum balance relationship with the inclusion of losses (Equation A13). Enthalpy h_7 is likewise calculated using an energy balance equation (Equation A14)

$$v_7 = \frac{c_l(\dot{m}_1 v_4 + \dot{m}_5 v_6)}{\dot{m}_1 + \dot{m}_5} \quad (\text{A13})$$

$$h_7 = \frac{\dot{m}_1 \left(h_4 + \frac{v_4^2}{2} \right) + \dot{m}_5 \left(h_6 + \frac{v_6^2}{2} \right)}{\dot{m}_1 + \dot{m}_5} - \frac{v_7^2}{2} \quad (\text{A14})$$

Within the constant area mixing section (Point 7-8), shock waves occur that compress and decelerate the flow to subsonic conditions. Flow property are determined by iterating

the density ρ_8 until it satisfies the conditions for the continuity, momentum, and energy Equations A15, A16 and A17. The iteration will continue until $\rho_8 = \rho'_8$ and pressure and enthalpy obtained is used to calculate the other fluid properties (Equation A18)

$$v_{8|\rho_8} = \frac{v_7 \rho_7}{\rho_8} \quad (\text{A15})$$

$$p_{8|\rho_8} = p_7 + v_7^2 \rho_7 - v_{8|\rho_8}^2 \rho_8 \quad (\text{A16})$$

$$h_{8|\rho_8} = h_7 + \frac{v_7^2}{2} - \frac{v_{8|\rho_8}^2}{2} \quad (\text{A17})$$

$$\rho'_{8|\rho_8}, s_{8|\rho_8}, T_{8|\rho_8} = f(p_{8|\rho_8}, h_{8|\rho_8}) \quad (\text{A18})$$

At the ejector exit (point 9), the mixture is further decelerated in the diffuser and pressure increases. The properties at the diffuser exit are determined by using the steady one-dimensional incompressible continuity equation (Equation A19). Velocity after the diffuser v_9 is calculated as

$$v_9 = v_8 \left(\frac{A_8}{A_9} \right) \quad (\text{A19})$$

The velocity is then used to calculate the enthalpy at ejector exit using Equation A20. The rest of the properties at ejector exit are calculated assuming constant entropy between the shock wave and the diffuser ie $s_8 = s_9$.

$$h_9 = h_8 + \frac{v_8^2}{2} - \frac{v_9^2}{2} \quad (\text{A20})$$

Appendix B Ejector fabrication

Ejector nozzle

1. The supersonic ejector was sized using the analytical model.
2. It was then 3-D printed from aluminium.

Ejector body parts

1. Solid stainless-steel shaft to the required outer diameter.
2. The shaft was bored with to the required CAMS diameters.
3. The shaft was drilled using tapered drill-bits to form the suction chamber end and the diffuser end.
4. Matching stainless-steel flanges were procured.

Ejector assembly

1. Ejector parts were welded together using fusion welding.
2. Secondary inlet was added.
3. A hole for pressure senser into the suction chamber was added.



Fig B1 Machine and cut stainless-steel shaft



Fig B2 Bored shaft for respective CAMS



Fig B3 Bored section with suction chamber and diffuser added

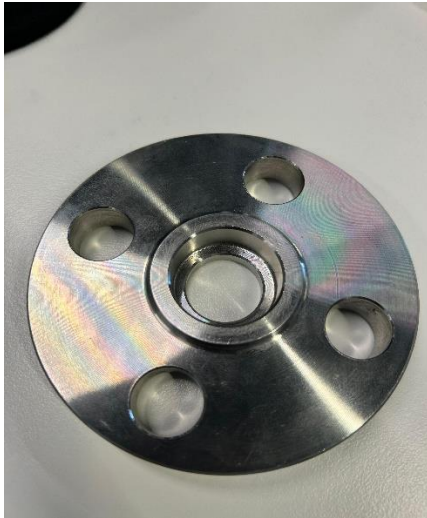


Fig B5 Stainless-steel flange

Fig B4 Primary and secondary flow sections ready for welding



Fig B6 Primary flow section welded to flanges



Fig B7 Complete ejector body



Fig B8 3-D printed nozzle

